Pressure-induced Structural Modifications and Amorphization of $CaGeO_3$-wollastonite, $MgGeO_3$-high-clinoenstatite and Mg_2GeO_4-olivine.

$CaGeO_3$ 準輝石, $MgGeO_3$ 輝石, Mg_2GeO_4 橄欖石の圧力誘起構造変化と非晶質化

1995

永井隆哉

(1)

Pressure-induced Structural Modifications and Amorphization of $CaGeO_3$-wollastonite, $MgGeO_3$-high-clinoenstatite and Mg_2GeO_4-olivine.

$CaGeO_3$準輝石, $MgGeO_3$輝石, Mg_2GeO_4橄欖石の圧力誘起構造変化と非晶質化

Doctoral Thesis

Presented to University of Tokyo

1995

Takaya Nagai

永井 隆哉

Contents

Abstract

In-situ X-ray diffraction measurements of $CaGeO_3$-wollastonite, $MgGeO_3$-high-clinoenstatite and Mg_2GeO_4-olivine were made using a diamond anvil cell under high pressure at room temperature, in order to gain better understanding of the metastable structural modification in the process of compression at kinetically low temperature. The measurements of $CaGeO_3$-wollastonite under high pressure and high temperature were also performed using a cubic anvil type apparatus (MAX80) installed in the National Institute for High Energy Physics in Tsukuba.

$CaGeO_3$-wollastonite is transformed into the rhodonite structure at about 6 GPa. $CaGeO_3$-rhodonite can be quenched at ambient pressure. The measured densities are in good agreement with the calculated density of hypothetical $CaGeO_3$-rhodonite. The phase with a modified perovskite structure is observed above 15 GPa and is transformed into the ordinary orthorhombic perovskite-form of $CaGeO_3$ in the decompression process from 27 GPa.

$MgGeO_3$-high-clinoenstatite converts to a phase with unidentified diffraction pattern at about 23 GPa. This new phase is regarded as none of the ilmenite-form, the $LiNbO_3$-form and the perovskite-form. This unidentified phase is reversibly transformed into the high-clinoenstatite-form at ambient pressure.

All the diffracted peaks of Mg_2GeO_4-olivine disappear in the pressure range from 25 GPa to 30 GPa. This pressure-induced amorphization is firstly confirmed by *in-situ* observation below about 30 GPa at room temperature. The amorphous state can be quenched under ambient condition, judging from the X-ray diffraction measurements in the decompression process.

The coordination change of germanium atoms occurs on the three

germanates under high pressures, as previously observed. The coordination change leads to a pressure-induced amorphization of Mg_2GeO_4-olivine. In contrast, some diffraction peaks of the high pressure phases with six-fold coordinated germanium atoms of $CaGeO_3$-wollastonite and $MgGeO_3$-high-clinoenstatite can be observed with increasing pressure before all diffraction peaks of their low pressure phases disappear.

These evidences are interpreted that the pressure-induced amorphization is a precursor phenomenon of the transition to a high pressure phase and that the balance (or competition) of the following two factors determines the appearance of "X-ray amorphous" state: (1) The conversion rate of the structural transition accompanied by the modification of the local structure in a low pressure phase. This modification is related to the coordination change of the Ge atoms. (2) The nucleation and growth rate of a high pressure phase, which is controlled by topological relation of the crystal structure between a low pressure and a high pressure phase. This interpretation is likely to be applied to the structural modifications in metastable compression of germanates and silicates at kinetically low temperature, when the coordination change of Ge atoms or Si atoms becomes a major mechanism of compression.

1. Introduction

General

When all the X-ray diffraction lines of crystalline substances disappear under high pressure, we judge that a pressure-induced amorphization occurs. Since the discovery of the pressure-induced amorphization of hexagonal ice (Mishima et al., 1984), the structural behavior of crystalline materials, under high pressure at kinetically low temperature, has been a subject of great interest not only in the field of material sciences but also of geophysical science. The kinetically low temperature means that the temperature is low enough to inhibit the transformation into a thermodynamically stable phase under high pressure.

For the last decade, it has been reported that the many crystalline substances show the pressure-induced amorphization (*e.g.* SnI_4 : Fujii et al., 1985 , $AlPO_4$: Kruger et al., 1990, $LiKSO_4$: Sankaran et al., 1988, $Ca(OH)_2$: Meade et al., 1992). It seems to be interesting and important evidence for the mechanism of a pressure-induced amorphization that some materials show reversible crystalline-amorphous transition and some do not. For example, $AlPO_4$ and $Ca(OH)_2$ show the reversible transition and can memorize even a crystal orientation.

It is well known that quartz and feldspar commonly are observed to have been converted to amorphous phases by the shock waves at relatively low temperature (Milton and De Carli, 1963). Recently several crystalline compounds, particularly on geophysically significant materials and its related materials, are known to undergo a vitrification by static compression at room temperature (cf. α-quartz : Hemly et al., 1988, α-quartz-type of GeO_2 : Yamanaka et al., 1992b, Wolf et al., 1992, Itie et al., 1989, fayalite : Williams et al., 1990, Richard and Richet, 1990, olivine structure compounds : Goyot and

Reynard, 1992, anorthite : Williams and Jeanloz, 1989, serpentine : Meade and Jeanloz, 1991).

Several interpretations have been proposed for the mechanism of the pressure-induced amorphization. Mishima et al. (1984) was interested in the relation between the pressure-induced amorphous phase and that of the so-called 'glass state' on the basis of their studies of ice at 77 K and 1 GPa. They suggested that the crystalline to amorphous transition under high pressure is a 'melting' phenomena, because an ice has a negative dT/dP slope on melting curve around room temperature at various pressures and the amorphization pressure seems to be correspond to the pressure where an extrapolated liquidus line is intersected. However, the pressure-induced vitrification of α-quartz, quartz-form of GeO_2, fayalite and anorthite, shows no evidence that their melting curves display a negative Clapeyron slope and/or have a maximum. Therefore, it seems that their interpretation as a high pressure 'melting' phenomena may not apply to these materials.

Various experimental approaches have been performed from the crystal chemical aspects for α-quartz and quartz-form of GeO_2 (Hemly et al., 1988, Hazen et al., 1989, Tsuneyuki et al., 1989, Itie et al., 1989, Yamanaka et al., 1992b, Wolf et al., 1992). According to their single-crystal X-ray diffraction experiments on α-quartz at high pressures, Hazen et al. (1989) indicated that the arrangement of the oxygen atoms approaches to a close-packed configuration with increasing pressure and when bending of all Si-O-Si angles become less than 120°, structural instabilities result in its gradual transition to an amorphous state. Itie et al. (1989) suggested from XAFS experiments that the coordination change from fourfold to sixfold under compression leads to the pressure-induced amorphization. The TEM observation by Wolf et al. (1992)

indicated that the stable region of the rutile-form GeO_2 , which is a high pressure stable phase coexist with quartz-form region and that size of the randomly oriented crystallites are too small to be coherent for X-ray diffraction. Based on a molecular dynamics (MD) simulation, Tsuneyuki et al. (1989) demonstrated that the amorphous state comprises mixed arrays of fourfold and sixfold Si-O coordination. Yamanaka et al. (1992b) described that the pressure-induced amorphization is a precursor phenomenon of the transformation to a high pressure thermodynamically stable phase, on the basis of the amorphization of GeO_2. However, the mechanism of the pressure-induced amorphization has been controversial yet and it is necessary to conduct more systematic researches so as to understand the relationship between the transition mechanism and the crystal structure.

Review to geophysical problems

As mentioned above, some geophysically significant minerals undergo a pressure-induced amorphization. However, there have been a few discussions on applications to geophysical phenomena.

Meade and Jeanloz (1991) first discussed geophysical significance of a pressure-induced amorphization. They observed acoustic emissions, which is a laboratory scale miniature of an earthquake, associated with a pressure-induced amorphization of serpentine [$Mg_3Si_2O_5(OH)_4$]. Because the temperatures achieved in subduction slub may remain below the dehydration temperature of serpentine until great depth, it is likely that the crystals of serpentine are metastably compressed inside the mantle and that it may undergo a pressure-induced amorphization within the subduction slub without the dehydration. Therefore, they infer that the acoustic emission in serpentine during the

amorphization may also be source for deep focus earthquake in the mantle.

According to high pressure and temperature experiments on quartz-form of GeO_2, Yamanaka et al. (1992b) indicated that once crystalline substances transform to a pressure-induced amorphous state, it is difficult to recrystallize. Yamanaka (1994) speculated that a pressure-induced amorphous phase is hard to recrystallize without extremely large thermal energy, therefore, if a pressure-induced amorphization occurs in cool subduction slub, the amorphous phase persists until great depth in the mantle. Meade and Jeanloz (1991) also suggested that a pressure-induced amorphous phase of hydrous minerals without dehydration become important water sources in the mantle. And it may explain 670 km discontinuity of deep focus earthquake, because the pressure-induced amorphous phase seem to be more ductile than crystalline substances.

Especially more investigations for mantle minerals, for example, olivine, pyroxene and their high pressure phases, are required to make clear the relation between a pressure-induced amorphization and mantle dynamics, such as deep focus earthquake and recycling water.

Present approaches

It is of great interest to investigate the possibility and the mechanism of a pressure-induced amorphization of mantle minerals. In this study the author focused on $CaGeO_3$, $MgGeO_3$ and Mg_2GeO_4, whose structures are the wollastonite-form, the high-clinoenstatite-form (*C2/c*) and the olivine-form, respectively, under ambient conditions. These germanates have been investigated as good analogous materials on various physical properties and phase transitions. Because these three germanates show similar polymorphic transitions at lower pressures in comparison with the corresponding silicates,

which are dominant minerals in the upper mantle.

Their structures are characterized by the approximately close-packed arrangement of the oxygen atoms; the first two germanates having a cubic close packing structure and the Mg_2GeO_4-olivine having a hexagonal close packing structure. The arrangement of the oxygen atoms of α-quartz-type compounds is far from close-packing but approaches to the close-packing with increasing pressure (Hazen et al., 1989). It is probable that the compression mechanism of these compounds having a close-packed oxygen framework is different from that of α-quartz and/or GeO_2.

Andrault et al. (1992) suggested on the basis of their XAFS studies that the pressure-induced coordination change occurs from about 7 GPa for $CaGeO_3$ and from about 8.5 GPa for $MgGeO_3$. Then, they speculated that the coordination change leads to a pressure-induced amorphization. In the case of quartz-type of GeO_2, pressure-induced coordination change results in the formation of nucleuses of rutile-form of GeO_2, but the size of nucleus is too small to be coherent for X-ray wave length, resulting in no diffraction. However, it is doubtful that same mechanism as proposed for GeO_2 also acts on compression process of $CaGeO_3$ and $MgGeO_3$, because their crystal structures are basically different from quartz-form of GeO_2, as mentioned in the previous paragraph. Guyot and Reynard (1992) reported that Mg_2GeO_4 is transformed to amorphous state at about 40 GPa. Since their results were based on the TEM observations, it is probable that the amorphous state may be produced as a result of a sufficient number of defects which were introduced into its crystal structure during the decompression process, as found in the $CaSiO_3$-perovskite. Therefore, it is greatly important to perform *in-situ* X-ray diffraction measurements under high pressure.

Therefore, the purpose of this study is to verify the possibility of the pressure-induced amorphization of these three materials and to make clear the relation of their crystal structures to the structural modifications under high pressure at kinetically low temperature by *in situ* X-ray diffraction measurements using diamond anvil cells with a conventional X-ray source and a cubic anvil type device (MAX80) with synchrotron radiation.

2. Phase relations and crystal structures

2.1 $CaGeO_3$

Phase diagram of $CaGeO_3$ is illustrated in Fig. 1. The $CaGeO_3$-wollastonite is stable under ambient pressure and temperature. With increasing pressure, tetragonal garnet form becomes stable and subsequently the garnet form is transformed into the orthorhombic perovskite form (cf. Prewitt and Sleight, 1969; Sasaki et al., 1983; Susaki et al., 1985; Ross et al., 1986).

Liebau (1960) reported that the wollastonite-form of $CaGeO_3$ is triclinic and belongs to space group $P\bar{1}$. Fig. 2(a), (b) show the illustrations of the wollastonite structure. The arrangement of the oxygen atoms approximates close packing in a rude way. Octahedrally coordinated Ca atoms alternate with tetrahedrally coordinated Ge atoms between the oxygen layers. The GeO_4 tetrahedra are linked as a one dimensional chain and the unit of the periodicity is three tetrahedra. The chains are oriented parallel to the *b*-axis (cf. Peacor and Prewitt, 1963).

2.2 $MgGeO_3$

Fig. 3 shows a schematic phase diagram of $MgGeO_3$. It has been a problem concerning $MgGeO_3$ structure, which is stable under ambient conditions, the clino-form or the ortho-form. However, Yamanaka et al. (1985) confirmed that the clino-form is stable under ambient conditions and the ortho-form is a high temperature form of $MgGeO_3$. With increasing pressure, the ilmenite-form is the first stable phase and then transforms into the corundum-form (cf. Ringwood and Seabrook, 1962, Kirfel and Neuhaus, 1974). Liu (1977) reported that the perovskite-form as a post corundum-form. However, his assumption was not confirmed by Ito and Matsui (1979).

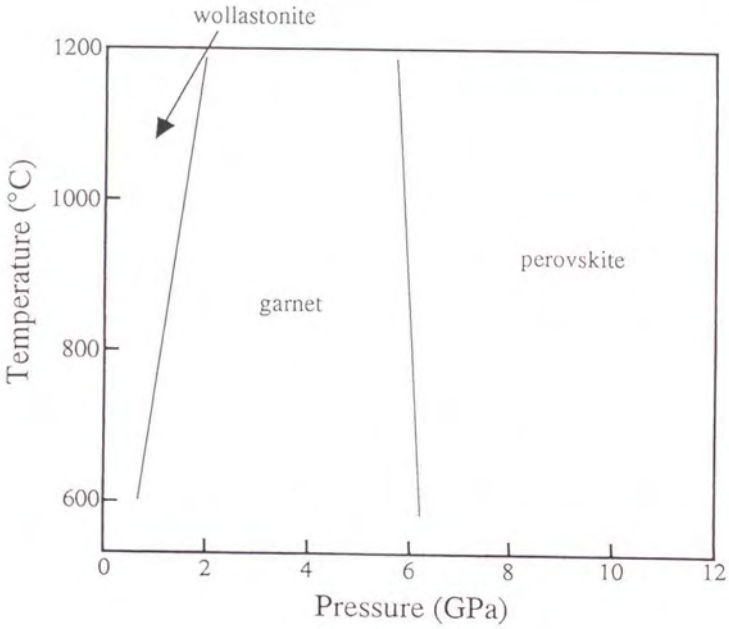

Fig. 1. Phase diagram of $CaGeO_3$.
This phase diagram was compiled by Liu and Bassett (1986).

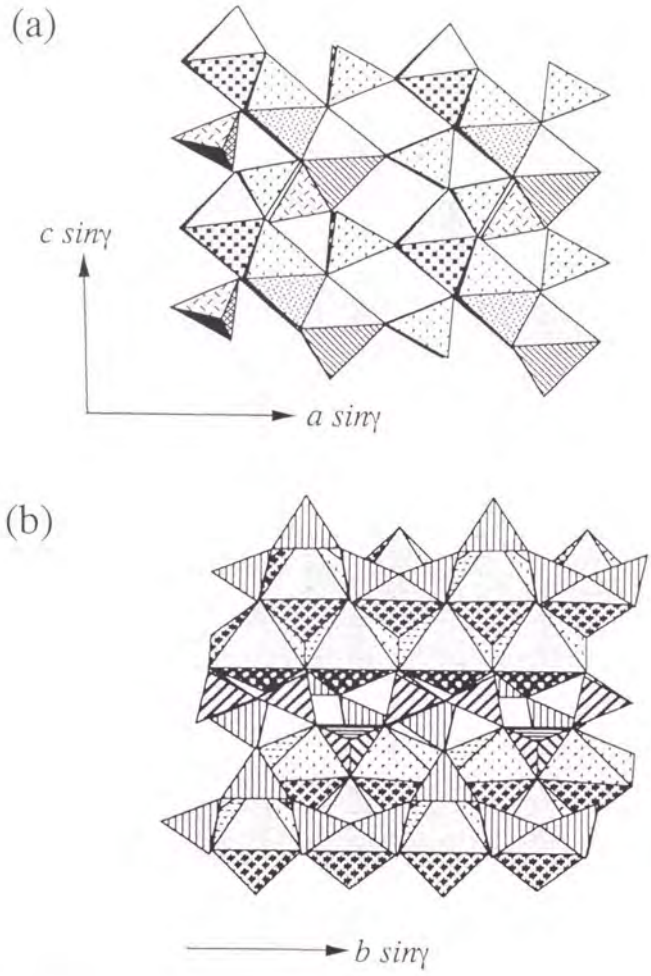

Fig. 2(a), (b). Crystal structure of $CaGeO_3$-wollastonite.
(a) Projection almost along the *b* axis of the structure of $CaGeO_3$-wollastonite is shown schematically. The alternation of octahedrally coordinated Ca atoms and tetrahedrally coordinated Si atoms is clearly observed.
(b) Projection on (101) plane. The repeat units of one dimensional chain of GeO_4 tetrahedra is three and the chains are oriented parallel to the *b* axis.

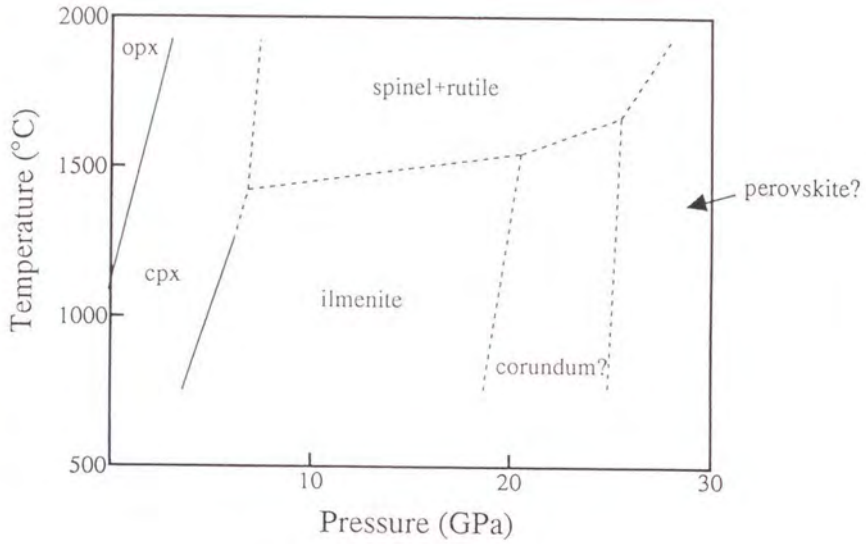

Fig. 3. Phase diagram of $MgGeO_3$.
This phase diagram was compiled by Liu and Bassett (1986).
The ortho-clino phase boundary was modified by Ross and Navrotsky (1988).

Recently Leinenweber et al. (1994) claimed that a high pressure form subsequent to the ilmenite-form is not the corundum-form, but is the lithium niobate form. And the perovskite polymorph formed from the lithium niobate phase of $MgGeO_3$ at room temperature and at 12-14 GPa by pressure-induced phase transition. The perovskite-form of $MgGeO_3$ remains to be uncertain.

Fig. 4(a), (b) illustrate of the high-clinoenstatite structure. Yamanaka et al. (1985) refined the crystal structure of the monoclinic phase of $MgGeO_3$, which has the arrangement of the oxygen atoms in a more ideal cubic closest packing than orthorhombic phase. Octahedrally coordinated Mg atoms alternate with tetrahedrally coordinated Ge atoms between the oxygen layers which are parallel to (100). The GeO_4 tetrahedra form one dimensional chains parallel to the *c*-axis.

2.3 Mg_2GeO_4

A schematic phase diagram of Mg_2GeO_4 is shown in Fig. 5. The phase relation of the Mg_2GeO_4 polymorphs has been discussed by many workers (*e.g.* Goldschmidt, 1931; Ringwood, 1956; Hensen, 1977; Will and Lauterjung, 1987), because Bernal (1936) suggested that Mg_2GeO_4 showed the same phase transition as $(Mg,Fe)_2SiO_4$ under relatively low pressure and temperature. However, Mg_2GeO_4 has a thermodynamically stable phase of the spinel form under normal conditions, but not the olivine form. And with increasing pressure, the spinel form decomposes into the mixture of the ilmenite-form $MgGeO_3$ and MgO (Liu,1977)

Fig. 6 shows the illustration of the olivine structure. Mg_2GeO_4-olivine is in an orthorhombic form with space group *Pbnm*. The arrangement of the oxygen atoms approximates a hexagonal close packing (HCP). The GeO_4

tetrahedra are isolated and Mg atoms occupy octahedral interstices of the HCP structure (cf. Hazen, 1976, Kudoh and Takeuchi, 1985, Will and Lauterjung, 1987).

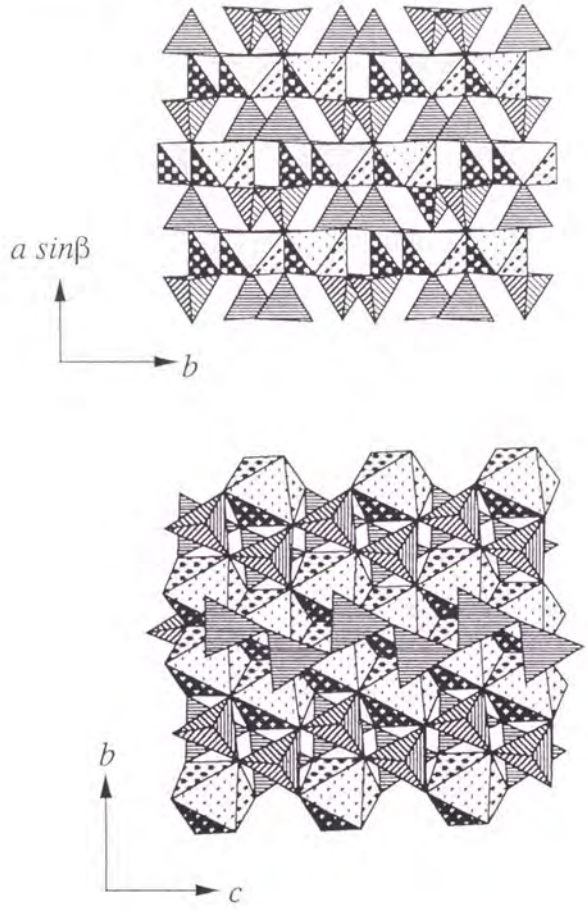

Fig. 4(a), (b). Crystal structure of $MgGeO_3$-high-clinoenstatite.
(a) Projection on the *b*-*c* plane of the structure of $MgGeO_3$-high-clinoenstatite is shown schematically. Chains composed of the GeO_4 tetrahedra are regularly arranged.
(b) Projection along the *b* axis. The alternation of octahedrally coordinated Ca atoms and tetrahedrally coordinated Si atoms is clearly observed.

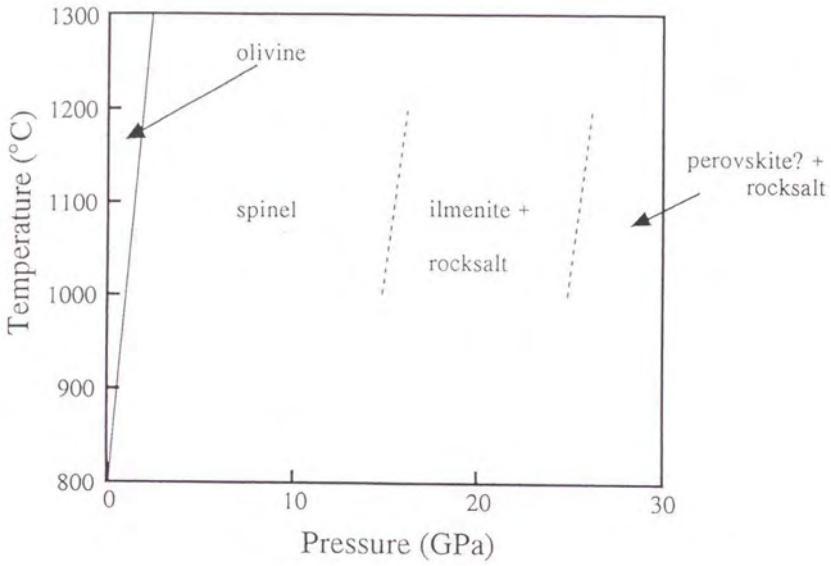

Fig. 5. Phase diagram of Mg_2GeO_4.
This phase diagram was compiled by Liu and Bassett (1986).

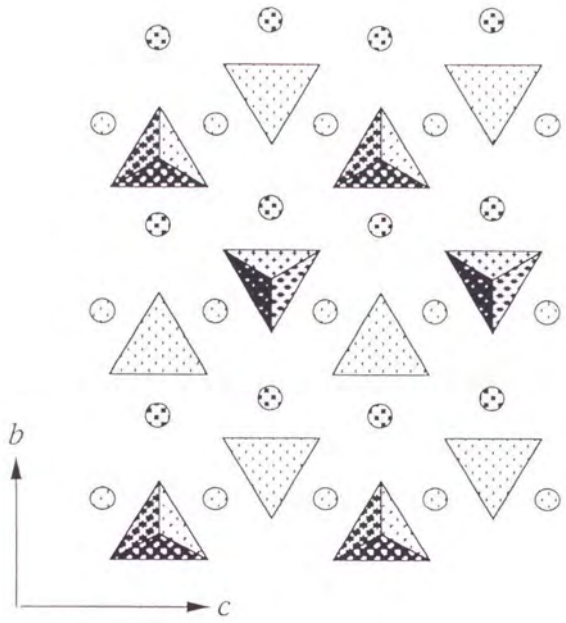

Fig. 6. Crystal structure of Mg_2GeO_4-olivine.
Projection along the *a*-axis. The GeO_4 tetrahedra are isolated.

3. Experimental procedures

3.1 *Sample preparation*

$CaGeO_3$ Powdered sample of $CaGeO_3$-wollastonite was prepared from an equimolar mixture of reagent-grade powders of $CaCO_3$ and GeO_2 by heating at 1473 K for 72 hours. A powder X-ray diffraction pattern of the product showed a single phase $CaGeO_3$-wollastonite.

$MgGeO_3$ Powder sample of monoclinic phase of $MgGeO_3$ with space group *C2/c* ($MgGeO_3$-high-clinoenstatite) was synthesized by the following way. At first an equimolar mixture of reagent-grade powders of MgO and GeO_2 was heated at 1473 K for 48 hours and then loaded at about 6 GPa and 727 K for an hour. High pressure syntheses were performed by a cubic anvil type apparatus installed at our laboratory. The cell assembly is shown in Fig. 7. The powder X-ray diffraction pattern of the product showed a single phase of $MgGeO_3$-high-clinoenstatite.

Mg_2GeO_4 Powder sample of Mg_2GeO_4-olivine was synthesized from regent-grade powders mixture of MgO : GeO_2 = 2 :1 by heating at 1473 K for 48 hours. The powder X-ray diffraction pattern of the product showed a single phase Mg_2GeO_4-olivine.

3.2 *High pressure apparatus*

3.2.1 *Diamond anvil cell*

Two types of diamond anvil cells (DAC) were used in this study. One (MK-40, Shimizu Seisakujo Co. Ltd.) was originally designed by Yamaoka et al. (1979) and was modified by our group in order to attach the goniometer head, which is shown in Fig. 8. A mounting disk is made of hardened steel with a conical opening of 60° for incident X-ray beam and another mounting disk

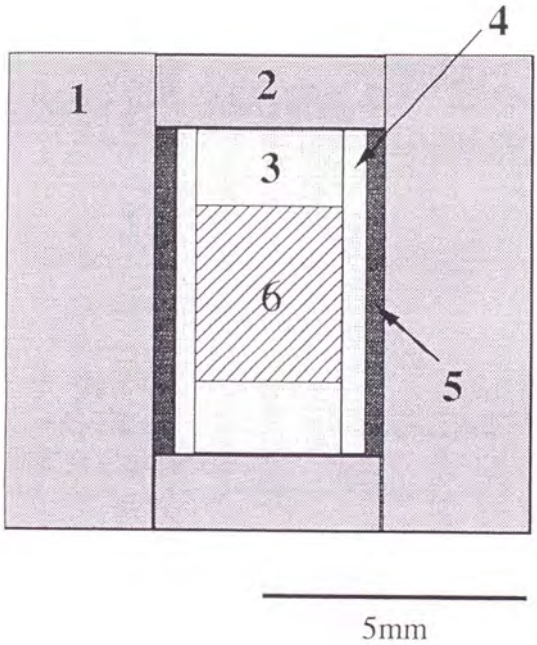

Fig. 7. Cell assembly of syntheses of $MgGeO_3$-high-clinoenstatite.
1: pyrophyllite pressure medium; 2: pyrophyllite cap;
3: BN cap; 4: BN sleeve; 5: graphite heater;
6: sample enclosed in Pt.

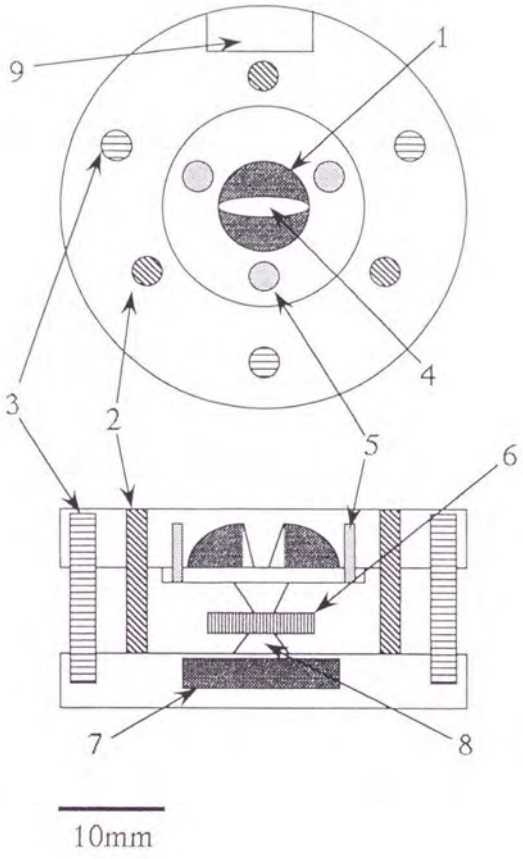

Fig. 8. Top and side views of cross sections of the MK-40 type DAC.
1: upper mounting disk; 2: stoppers; 3: tightening screws; 4: slit;
5: adjusting screw for mounting disk; 6: gasket; 7: lower mounting disk;
8: diamond anvil; 9: groove for an attachment jig of a goniometer .

has a slit opening of 90° for X-ray powder diffraction. About 0.125 ct diamonds with 0.5 mmϕ culet were used. Powdered sample with a few ruby chips was loaded in the 0.3 mm diameter hole of a stainless steel (SUS304) gasket which was initially 0.3 mm thick and preindented to 0.15 mm thick. The 4 : 1 mixture of methanol : ethanol was used as a pressure medium to generate reasonable hydrostatic pressure. All operations were performed under a microscope. The DAC is cramped to maintain the desired pressure after a pressure generation.

Another type of DAC was a lever-and-spring type DAC (Toshiba Tangaroi Co. Ltd.), which is shown in Fig. 9. This type of DAC was originally designed by Mao and Bell (Mao and Bell, 1978) and the alignment system of diamonds was modified by Prof. Yagi (Yagi et al., 1982). About 0.29 ct diamonds with 0.5 mmϕ culet were used. Sample loading and gasket were the same as mentioned above. Argon gas was used as a pressure medium to generate reasonable hydrostatic pressure. Argon gas was loaded into sample chamber at room temperature by compressing it up to 0.1 GPa at the Institute for Solid State Physics, Univ. of Tokyo.

It is of great importance to adjust the two diamond faces parallel in order to generate high pressure stably. The opposed anvils were carefully aligned under a microscope until the Newton interference fringes seen between the two diamond faces become less than 1 in number.

The pressure was determined by usual method of measuring the shift of R1 fluorescence line of a ruby chip. Ar-ion laser beam was applied to the ruby chip beside the sample through the diamond anvil and the ruby R1 fluorescence emission is analyzed by a grating monochromator and converted to electrical signal by a photo multiplier. The ruby R1 fluorescence line is emitted with the

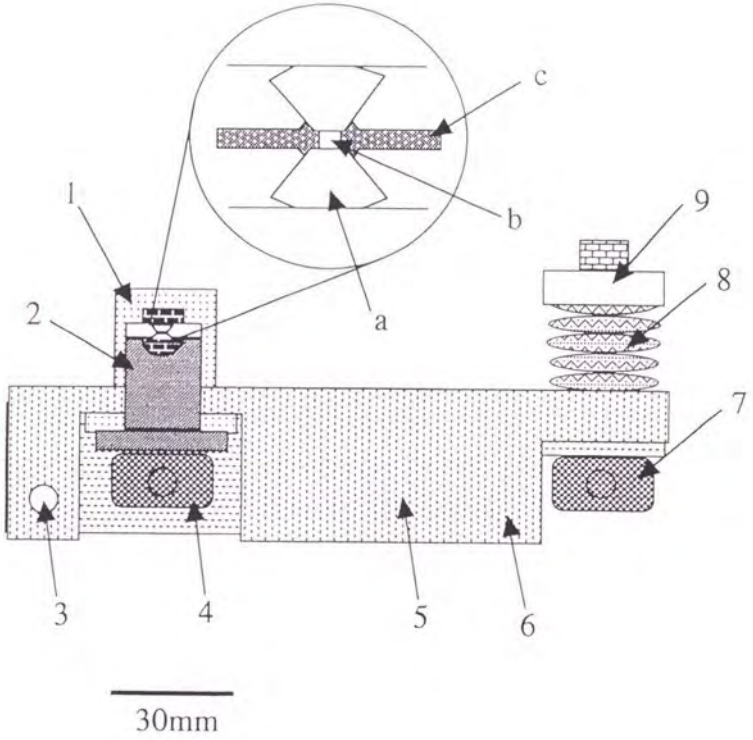

Fig. 9. Side view of cross section of the lever-and-spring type DAC.
1: cylinder; 2: piston; 3: fulcrum; 4: thrust block; 5: lever arms;
6: main body of the lever assembly; 7: spring holder;
8: Bellevile washers; 9: torque nut;
a: diamond anvil; b: sample chamber; c: gasket.

transition from an excited state of Cr^{3+} ion in α-Al_2O_3 to a ground state. The transition energy depends on the Cr-O distance in $[CrO_6]^{9-}$ clusters and the Cr-O distance depends on the pressure. Therefore, the generated pressure can estimated by measuring the shift of R1 ruby fluorescence line (Piermarini et al., 1975).

3.2.2 *Cubic anvil type device*

A cubic anvil type device installed at our laboratory. The cubic anvil type apparatus consists of six anvils made of tungsten carvide, four of which are fixed to the anvil blocks on a horizontal plane and the other two anvils located at the center of the upper and the lower pressing blocks advances vertically, when a hydraulic press works. The cell assembly is shown in Fig. 10. The pressure medium is made of pyrophyllite in order to generate reasonable hydrostatic pressure.

The magnitudes of pressure generated in the sample were calibrated by detecting the change of electric resistance of Bi (I-II) at 2.55 GPa and Ba (I-II) at 5.5 GPa. On the basis of the data, the relation between the load oil pressure in the hydraulic press of the apparatus and the pressure generated in the sample is estimated.

3.2.3 *Uniaxial split sphere type apparatus*

A uniaxial split sphere type apparatus installed at Institute for Study of the Earth's Interior (ISEI), Okayama Univ. in Misasa were used in order to obtain relatively large volume of $CaGeO_3$ powder sample recovered from the high pressures at room temperature. The summary of the construction of a uniaxial split sphere type apparatus is as follows. The cubic anvil assembly of

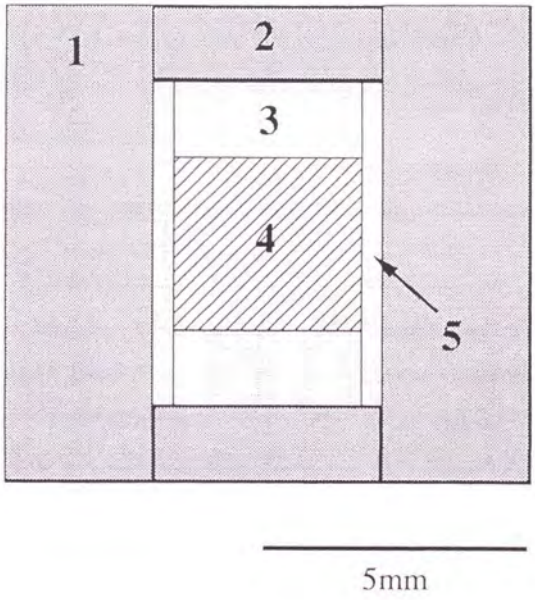

Fig. 10. Cell assembly of a cubic anvil type device.
1: pyrophyllite pressure medium; 2: pyrophyllite cap;
3: BN cap; 4: sample enclosed with Pt; 5: BN sleeve.

tungsten carbide is compressed with the aid of a press with power of 5,000 tons. One corner of each cubic anvil is truncated. The size of truncation is 3 mm. Therefore, the shape of the pressure medium is octahedron, which is made of semi-sintered MgO. The cell assembly is shown in Fig. 11.

The magnitudes of pressure generated in the sample were calibrated by detecting the change of electric resistance of Bi (I-II) at 2.55 GPa, Bi (III-V) at 7.7 GPa, ZnS (metalic) at 15.6 GPa and GaP at 23 GPa.

3.2.4 *MAX80*

A cubic anvil type apparatus, MAX80 (Shimomura et al., 1984, 1985 etc.) is installed at the beamline AR-NE5C at the National Institute for High Energy Physics (KEK). *In-situ* X-ray diffraction measurements can be performed under high pressure and temperature conventionally. In the present study sintered diamond anvils truncated 4×4 mm square and 7×7×7 mm^3 pressure medium made from the amorphous boron/epoxy resin were used. Because the absorption coefficient of the amorphous boron/epoxy resin is extremely small, it is a good pressure medium for *in-situ* X-ray diffraction experiments. The present cell assembly is shown in Fig. 12. Carbon disks were used as heaters and sample temperature was monitored by a almel-chromel thermocouple. A sample chamber was filled with $CaGeO_3$ powders and powder mixture of NaCl and BN. Before diffraction measurements of $CaGeO_3$ sample, an X-ray diffraction profile of the mixture of NaCl and BN was obtained in each time. The cell volume of NaCl was calculated from the values of 220 and 222 diffraction peak of NaCl at each pressure and pressure values were estimated on the basis of Decker's equation of state for NaCl (Decker, 1971).

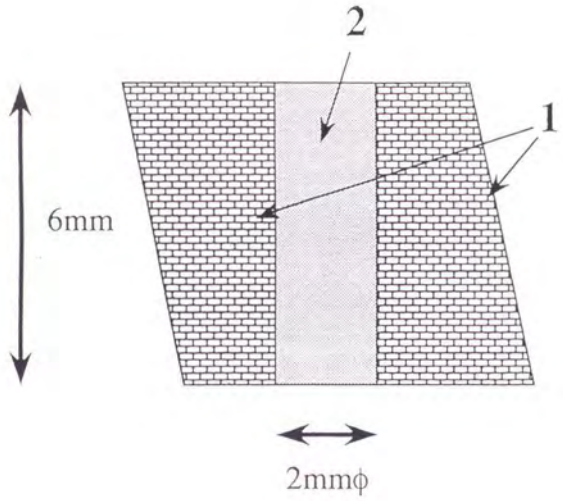

Fig. 11. Cell assembly of a uniaxial split sphere type apparatus.
1: magnesia pressure medium; 2: sample enclosed in Pt.

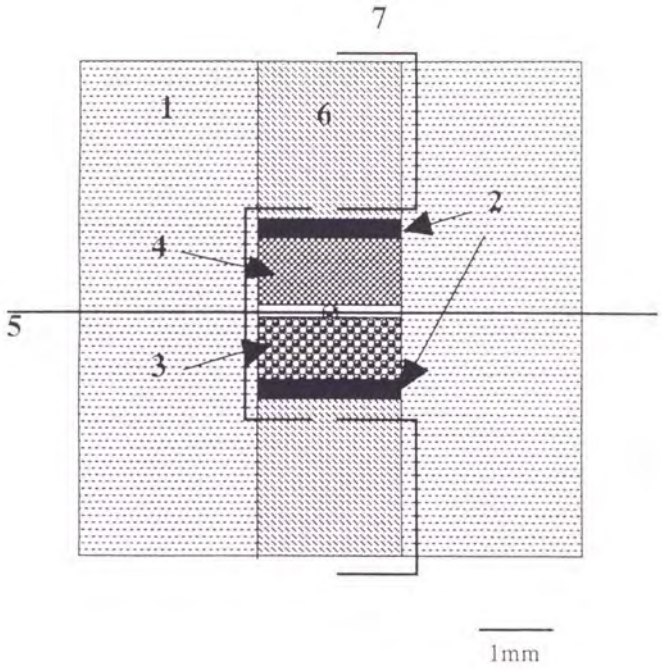

Fig. 12. Cell assembly (MAX80).
1: Boron epoxy pressure medium; 2: carbon disk heaters;
3: NaCl; 4: sample; 5: almel-chromel thermocouple;
6: pyrophyllite cap; 7: gold electrode.

3.3 *X-ray source and diffraction measurement systems*

3.3.1 *Yamanaka Lab. in Osaka Univ.*

In-situ X-ray diffraction measurements under high pressure by using the MK-40 type DAC by the angular dispersive method were conducted in Yamanaka Lab., Osaka Univ. by using a curved position sensitive detector (PSD, Inel CPS-120) as a detector and a Molybdenum-target rotating anode X-ray generator (Rigaku RU-200) as an X-ray source. Yamanaka et al. (1992a) described this system in detail. Summary of this system is as follows. The illustration of this system is shown in Fig. 13.

The PSD is a curved linear detector. The anode is a thin curved metal blade. The chamber is a section of a circular arc whose center is located at the powder and crystal sample. The radius of curvature is 250 mm and the angular aperture is 120°. The positioning of the X-ray photon is determined by the delay-line readout method. The chamber works in "self-quenching streamer" mode (Ballon et al., 1983) with a gas mixture of Kr (85 %) and C_2H_6 (15 %) and this mode realizes its high signal-noise ratio (S/N). The dynamical range is 10^5 cps and the angular resolution is 0.06° /2θ.

Signals from the PSD are amplified and/or shape-adjusted with both a pre- and a main-amplifier and then are converted to digital signals by a first A-D converter (450 MHz). Because the digital signals are forwarded to a histogram memory module at a forwarding speed of 1.2 μsec per a channel, dead time caused by data transfer is too short. The detector and goniometer are controlled by a personal computer through the computer aided measurement and control (CAMAC) system and IEEE-488 bus, respectively.

X-ray source is a Mo-target of a rotating anode X-ray generator and loading power was usually 50 kV and 180 mA. Incident X-ray beam was

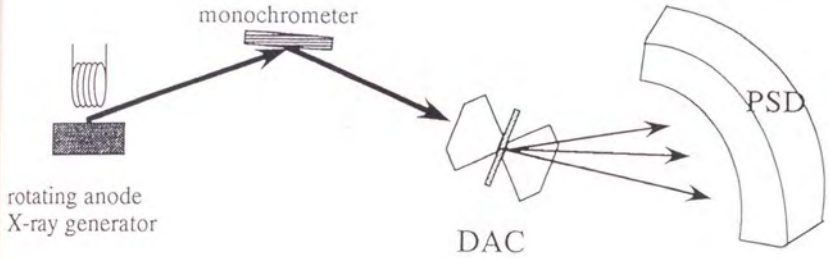

Fig. 13. Illustration of the X-ray diffraction measurements system installed in Yamanaka Lab., Osaka Univ..
Note: Position Sensitive Detector (PSD), Diamond Anvil Cell (DAC).

monochromatized by (002) reflection of pyrolytic graphite and a 0.1 mmϕ collimator was used.

3.3.2 *BL-4B in Photon Factory*

In-situ X-ray diffraction measurements by using a lever-and-spring type DAC were performed by the X-ray energy dispersive method at the beamline-4B in the Photon Factory (PF), the KEK. X-ray source is a high energy synchrotron radiation (2.5 GeV) from the electron/positron storage ring. SR X-rays have a continuous spectral distribution without any characteristic radiation formed in a conventional laboratory X-ray source and provides as with the highly brilliant radiation in the X-ray region. Synchrotron radiation (SR) is introduced into the beam-line from a bending magnet in the storage ring.

Many structural studies under high pressure have been made by using the X-ray energy dispersive method (*e.g.* Skelton et al., 1982). The energy dispersive method with SR has a great advantage for diffraction studies under high pressure such as phase determination and lattice-parameter measurement (*e.g.* Huang and Bassett, 1986), because the X-ray diffraction pattern of very small amount of sample in a DAC can be obtained within a very short time.

Incident white X-ray cut by a vertical and a horizontal slit (the width of both slits are 0.1 mm.) was led into the sample. Therefore no diffraction signal from a gasket was detected. And diffracted X-ray through both a solar slit and a 0.5 mm vertical slit were detected by an intrinsic Ge solid state detector (SSD). The DAC and the SSD were set on the diffractometer installed at the beamline-4B, which was designed for powder and molten-salt structure analyses (Ozawa et al., 1988). The DAC was installed at the center of a goniometer and

the SSD was fixed on 2θ-arm. The SSD was used to measure photons of energy in the range 10 to 40 keV. The angular position 2θ of the SSD was set so that all diffraction peaks appeared beyond the Ge *K*-absorption edge (11.103 keV). To take into consideration of both a slit opening of the DAC and the energy dependence of the counting efficiency of the Ge-SSD, the Energy dispersive spectra were taken with the SSD set at $2\theta = 6.02°$. Fig. 14 shows the schematic diagram of this system. The intensity data collection was made by the CAMAC system (Yamanaka et al., 1992b).

Calibration of the photon energy using a multichannel analyzer with 1024 channels was made by measuring the radiation from radio isotope Am. A linearity between the channel number and the energy was confirmed within 1 %. The dead time of the AD converter was kept within 5 % in order to lessen the effect of pile up.

3.3.3 *AR-NE5C in KEK*

In-situ X-ray diffraction measurements by using the MAX80 were performed by the X-ray energy dispersive method at the beamline-NE5C in the accumulation ring (AR) of the TRISTAN main ring, the KEK. An accelerating energy of SR from the AR is 6.5 GeV. SR is introduced into the beam-line from a bending magnet in the AR. As mentioned above, the energy dispersive technique using SR source has a great advantage for diffraction studies under high pressure.

Incident white X-ray beam cut by slits (a 0.2 mm vertical and a 0.2 mm horizontal slit) was led into the sample and diffracted X-ray through a 0.2 mm vertical collimator and slits (a 0.2 mm vertical and a 0.2 mm horizontal slit) were detected by a pure germanium solid state detector (Ge-SSD).

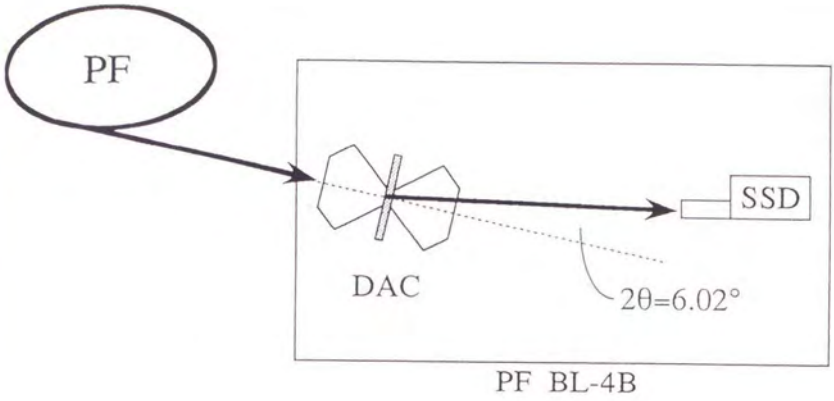

Fig. 14. Schematic diagram of the X-ray diffraction measurements system installed at beamline 4B in the PF.
Note: Solid State Detector (SSD).

In consideration of energy range of photons and energy dependence of counting efficiency of Ge-SSD, 2θ–angle was fixed at 3.8°. Fig. 15 shows the schematic illustration of this system. The Ge-SSD was used to measure photons of energy in the range of 20 to 130 keV. The intensity data collection was made by the CAMAC system.

Assignment of 1024 channels of a multichannel analyzer to the photon energy was made by the fluorescence of $K\alpha$ and $K\beta$ radiations of Cu, Rb, Mo, Ag and Ba elements in the form of foils. A linearity between the channel number and the energy was confirmed within 1 %.

3.4 *Density measurement system*

Density determination by the Archimedes' Principle was performed by using the Berman density torsion balance (Fig. 16) in Tsukuba University. In the case of density determination of a small sample volume, it is difficult to measure the volume directly. According to the Archimedes' Principle, the volume is determined by measuring the apparent loss in weight when a weighed mineral fragment is immersed in a CCl_4 liquid of known specific gravity. A CCl_4 liquid was used, because water has a high surface tension and does not wet solids readily. Bubbles were removed carefully, because bubbles are tenaciously held on the solid and the result in an erroneously low density determination. The fragment displaces an amount of liquid equal to its own volume and its weight is apparently diminished by the weight of the liquid displaced.

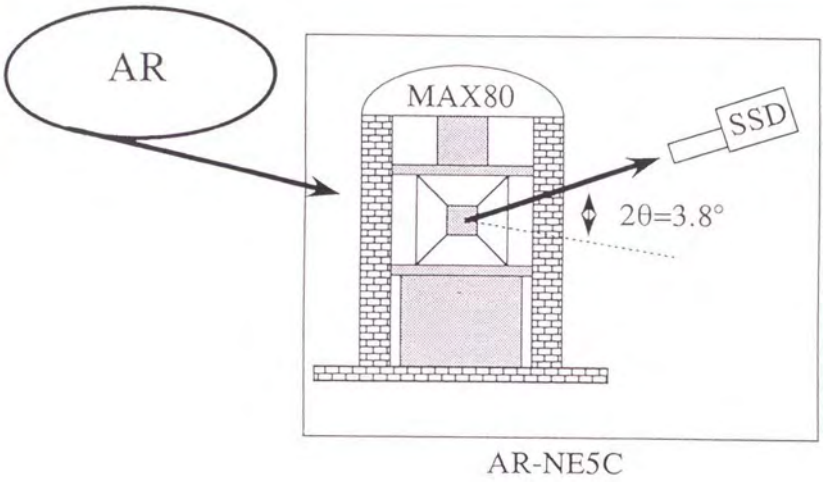

Fig. 15. Schematic diagram of the X-ray diffraction measurements system at beamline NE5C in the AR.

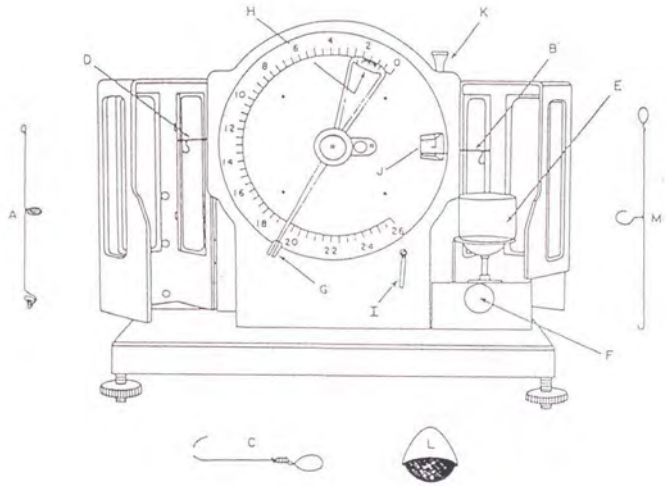

Fig. 16. Illustration of Berman density torsion balance.
A: double weighing pan, B: right end of beam,
C: counterweight, D: left end of beam, E: liquid dish,
F: turn knob, G: adjust index level, H: vernier,
I : beam clamp lever, J: balance pointer, K: adjustment knob,
L: basket, M: wire hook.

3.5 *Experimental conditions*

For the purpose of both investigating the structural change with increasing pressure and confirming a possibility of a pressure-induced amorphization, *in-situ* X-ray powder diffraction measurements at room temperature were performed for $CaGeO_3$ up to 27 GPa and for $MgGeO_3$ up to 35 GPa by the angular dispersive method using a MK-40 type DAC, the PSD and a rotating anode X-ray generator in our laboratory. Data collection for Mg_2GeO_4 was performed up to about 35 GPa at room temperature by the energy dispersive method using a lever-and-spring type DAC, the SSD and the SR X-ray source at the beamline 4B (BL-4B) in PF. Diffraction profiles of $CaGeO_3$ were measured by the energy dispersive method at about 6.8, 8.8 and 12.2 GPa with increasing temperature up to 600 °C by using the MAX80 installed at AR-NE5C in KEK, in order to observe the change of diffraction profiles during the transition from wollastonite structure to garnet structure and to perovskite structure. Therefore, X-ray diffraction data were collected until the temperature where garnet or perovskite phase appeared.

$CaGeO_3$ samples were recovered from 6, 20 and 26 GPa runs at room temperature so as to prepare the sample for density measurement. Only 6 GPa run was conducted by using the cubic anvil type device installed at our laboratory, other runs were performed by a uniaxial split sphere apparatus installed in ISEI. The density of these samples were measured by the Berman density torsion balance in Tsukuba Univ.. After density measurement, X-ray powder diffraction patterns were also obtained.

4. Results

4.1 *Characterization of starting materials*

It was confirmed that the synthesized starting materials of $CaGeO_3$-wollastonite, $MgGeO_3$-high-clinoenstatite and Mg_2GeO_4-olivine were single phases, on the basis of the data of X-ray powder diffraction measurements. The cell dimensions of the synthesized samples obtained by the least-squares refinements of the reflections are given in Table1.

4.2 *$CaGeO_3$*

4.2.1 *Diffraction profiles by DAC*

Diffraction profiles of $CaGeO_3$ obtained by *in-situ* X-ray diffraction measurements using MK-40 type DAC up to 27 GPa at room temperature (Fig. 17) showed that the profiles up to 27 GPa are composed of three stages. A plot of interplanar spacings *versus* pressures is shown in Fig. 18.

At the first stage observed up to about 6 GPa, all diffraction peaks of wollastonite-form shifted to relatively higher angle with increasing pressure, but no drastic change occurs. It suggests that $CaGeO_3$-wollastonite was compressed hydrostatically in this stage. The cell volumes were calculated from the cell dimensions determined up to 3.4 GPa by a least-squares method with 15 observed reflections. The V/V_0 ratios change with increasing pressure as shown in Fig. 19. Data were fitted with the Birch's equation of state,

$$P=3/2\times K_0\{(V_0/V_p)^{7/3}-(V_0/V_p)^{5/3}\}$$

where P is pressure, V_0 is the unit cell volume at 0.1MPa, V_p is the unit cell volume at pressure P and K_0 is the isothermal bulk modulus. The Birch's equation of state is derived from fixing the value of K_0' as 4 in Birch Mahnagan's equation of state.

Table 1. Summary of cell dimensions of the synthesized starting materials of $CaGeO_3$-wollastonoite, $MgGeO_3$-high-clinoenstatite and Mg_2GeO_4-olivine.

	$CaGeO_3$ wollastonite	$MgGeO_3$ high-clinoenstatite	Mg_2GeO_4 olivine
Space Group	$P\bar{1}$	*C2/c*	*Pbnm*
a (Å)	8.12(2)	9.597(1)	4.90(2)
b (Å)	7.55(2)	8.933(1)	10.29(2)
c (Å)	7.28(1)	5.158(1)	6.02(3)
α (°)	89.97(8)	90	90
β (°)	94.38(1)	100.99(1)	90
γ (°)	103.38(2)	90	90

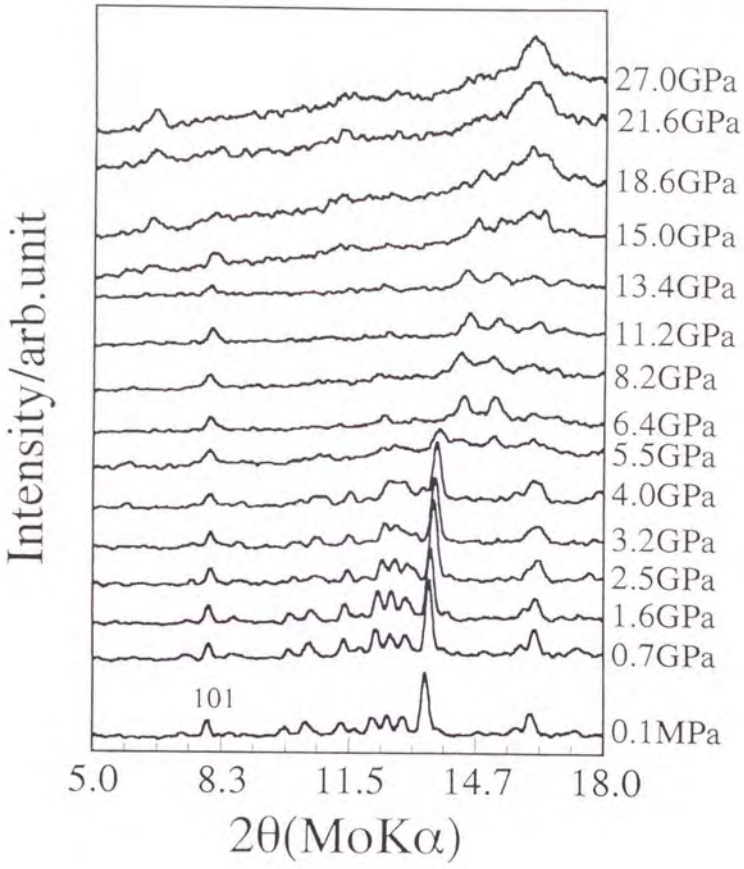

Fig. 17. X-ray diffraction patterns of $CaGeO_3$-wollastonite on compression up to 27 GPa.

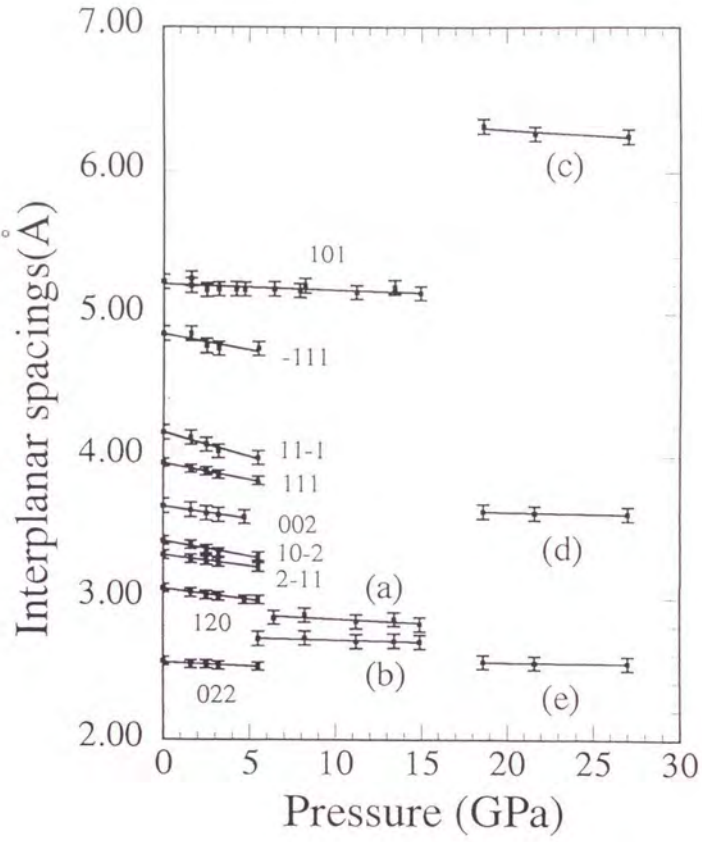

Fig. 18. Interplanar spacings *versus* pressure on $CaGeO_3$.
The symbols of (a) and (b) correspond to diffraction peaks appeared in the second stage. The symbols of (c), (d) and (e) correspond to diffraction peaks observed in the third stage.

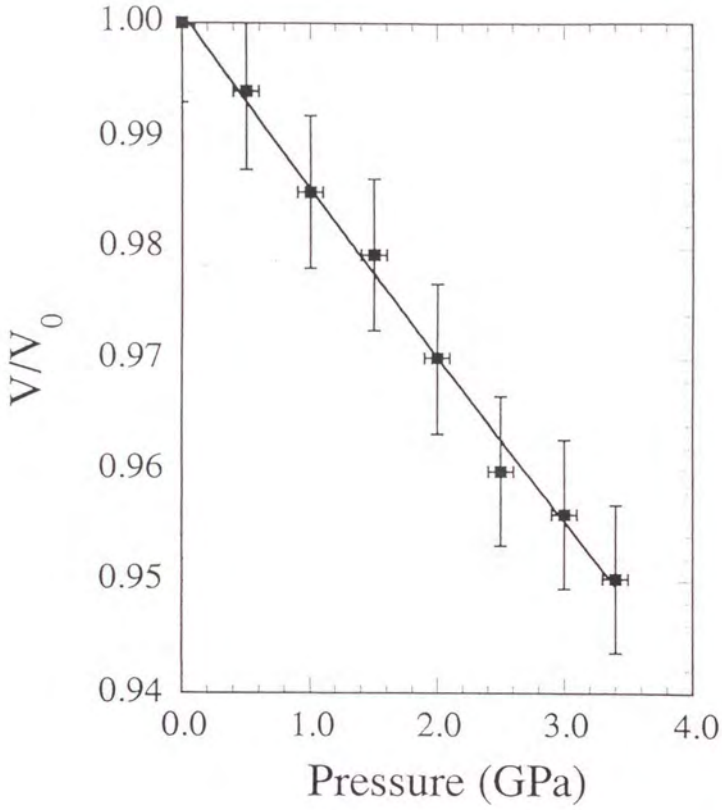

Fig. 19. Variation of V/V_0 with increasing pressure on $CaGeO_3$-wollastonite. A solid curve fitted by the Birch's equation of state.

The K_0 was determined to be,

$$K_0 = 83 \text{ GPa } (\pm 10 \text{ GPa})$$

This value includes large errors, because the number of reflections used in calculation of the cell volume is not sufficient, in spite of the low space group $P\bar{1}$. However, the value is in good agreement with the previously reported value K_0 (Liebermann, 1974) determined by measurements of elastic wave velocity under pressures. This result means that the present data provide a reliable measure of the bulk modulus of $CaGeO_3$-wollastonite.

The second stage starts at about 6 GPa. This stage is characterized by the appearance of at least two new observed peaks and the disappearance of almost all reflections of the wollastonite-form except the 101 reflection. The 101 plane of the wollastonite-form is parallel to close-packed oxygen layers. This evidence suggests that the oxygen layers are preserved and that the atomic displacement takes place between the oxygen layers. Two new peaks of 2θ =14.16(6)° and 14.94(5)° at 6.4 GPa are found together with the above 101 peak. It is clear that these peaks belong neither to the garnet-form nor to the perovskite-form. Both the garnet-form and the perovskite-form have been reported as high pressure stable phase of the wollastonite-form. Therefore, the wollastonite-form is transformed into a new phase at about 6 GPa.

The profile changes of the diffraction pattern shown with decreasing pressure from 14.9 GPa to ambient pressure (Fig. 20), indicate that the transformation from the wollastonite-form to a new phase is irreversible. X-ray diffraction profiles of the recovered samples obtained by a multianvil high pressure apparatus from 6, 10, 15, 20 and 26 GPa (Fig. 21) show the same trend as the profile of a new phase which is observed under compression in the DAC experiments. Accordingly, two strong diffraction peaks having

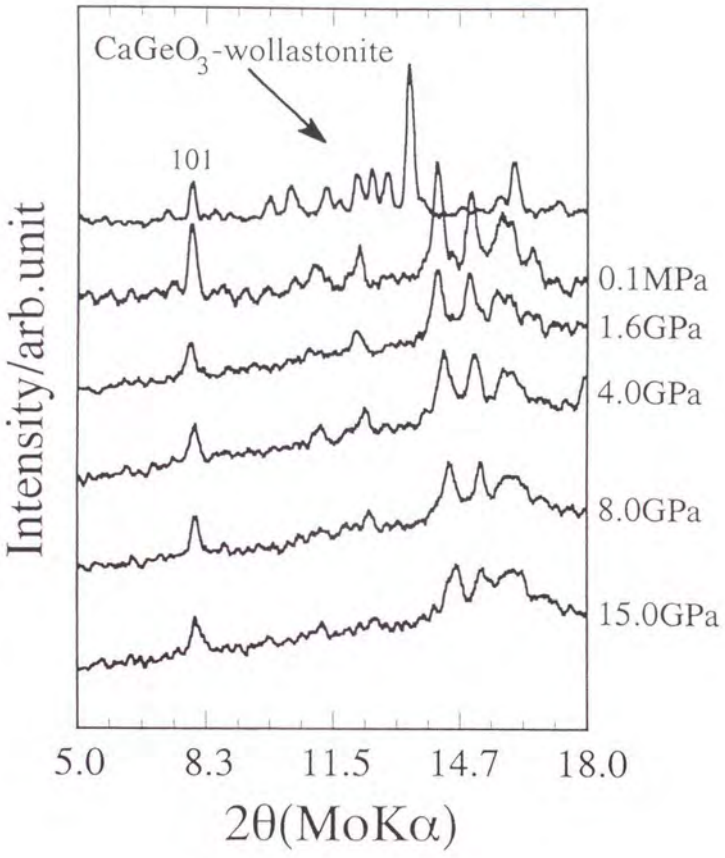

Fig. 20. X-ray diffraction patterns of $CaGeO_3$-wollastonite on decompression from 14.9 GPa.

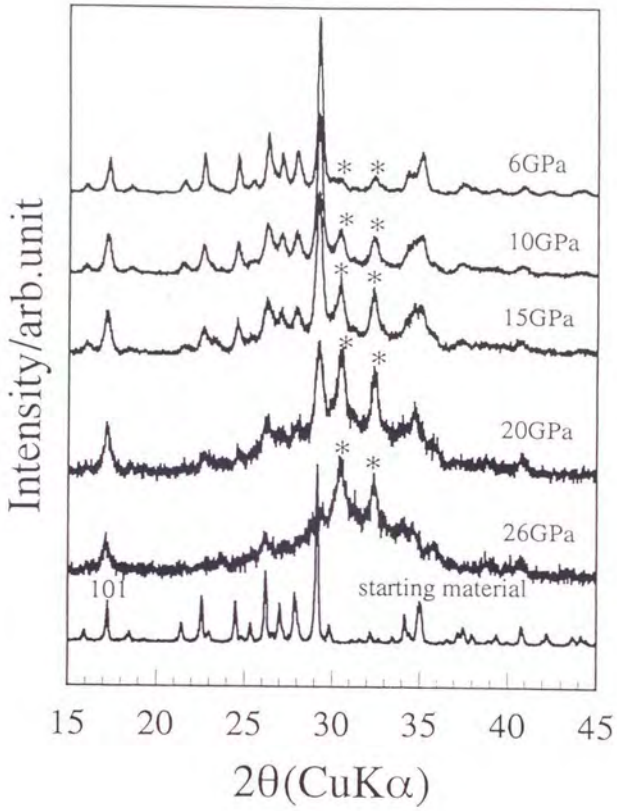

Fig. 21. X-ray diffraction patterns of recovered samples from 6 GPa, 10 GPa, 15 GPa, 20 GPa and 26 GPa. Two reflections marked by * have d=2.93 Å and 2.76 Å.

2θ=13.91(8)° and 14.78(5)° under ambient conditions can be observed remarkably. The X-ray diffraction profile of the recovered sample from 26 GPa run is similar to the profile of the second stage. However, the result of *in-situ* X-ray diffraction measurement suggests that the diffraction pattern at the pressure of 26 GPa corresponds to that of the third stage. This discrepancy may present that the onset pressure of the transition is related to hydrostatisity.

This new phase can be identified as the rhodonite structure. The rhodonite belongs to pyroxenoid group and the number of repeat units of GeO_4 tetrahedron in the chain pattern is five. $CaGeO_3$-rhodonite has never been reported before. A diffraction profile of a recovered sample from a high pressure (6 GPa) and a hypothetical simulated powder diffraction pattern are shown in Fig. 22. The simulation was performed on the basis of the structural parameters reported by Narita et al. (1977). It is clear that those two patterns resemble quite well. And the new two reflections appeared under pressure in the DAC experiments fit in with the two strongest reflections (2θ=13.91(8)° and 2θ=14.78(5)°) in the pattern of the rhodonite form of $CaGeO_3$.

As shown in Fig. 21, the diffuse haloes in the diffraction profile become remarkable with increasing the peak pressure at which the recovered samples experienced. It is suggested that the recovered sample includes not only $CaGeO_3$-rhodonite, but also an amorphous phase and the amorphous materials provide the diffuse haloes. And the ratio of the amorphous part to the crystalline one of the $CaGeO_3$-rhodonite increases as the pressure increases.

The profile change of the third stage starts at about 15 GPa. Two new different peaks clearly appear and a different broad but weak peak seems to enhance. The clear peaks have 2θ=6.39(8)° and 15.88(5)°, and the broad peak is around 2θ=11.0°~11.3° at 27 GPa. On the other hand, all other peaks

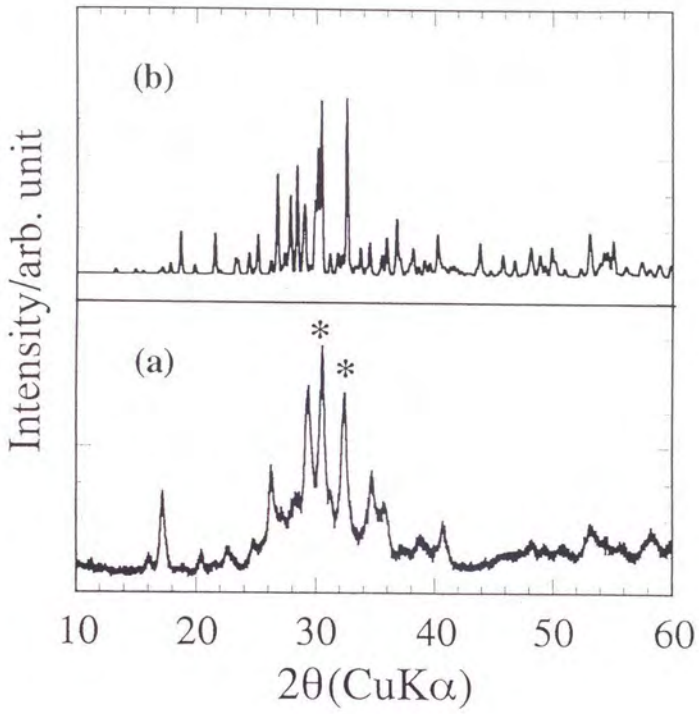

Fig. 22. (a) A diffraction pattern of a recovered sample from 6 GPa at 200 °C and (b) a hypothetical simulated powder pattern of $CaGeO_3$-rhodonite.
Two reflections marked by * have d=2.93 Å and 2.76 Å.

including the new peaks found in the second stage and the 101 reflection of the wollastonite-form is vanished above 20 GPa. These facts indicate that the structural framework changes and a new different phase appears. Only three peaks were observed at *d*-value=6.37(8) Å, 3.65(9) Å and 2.57(4) Å at 27 GPa.

As is shown in the X-ray diffraction profile of a recovered sample from 27 GPa (Fig. 23), two reflections having *d*=3.75(5) Å and 2.63(5) Å are preserved. And one peak having *d*=6.37(8) Å at 27 GPa disappears in decompression process. It is believed that the former two reflections correspond to 110 (or 002) and 112 (020 and 200 reflection are overlapped.) reflection of the perovskite-form of $CaGeO_3$, respectively. In addition some other reflections can be indexed as the perovskite-form. The reflections having *d*=1.86(2) Å, 1.52(2) Å and 1.31(2) Å are indexed as 220 (+004), 132 (+024, +204) and 224 reflections of the perovskite-form, respectively. The *d*-values under ambient conditions, which were calculated by the diffraction data of the recovered sample, are well consistent with that of the perovskite-form of $CaGeO_3$ (Table 2). It is concluded that the recovered sample from 27 GPa has the perovskite-form.

Since it has been reported that the perovskite-form of $CaGeO_3$ is a quenchable phase, the diffraction profiles above 15 GPa can be attributed to the perovskite structure. Sasaki et al. (1983) indicated that the perovskite-form of $CaGeO_3$ is psuedocubic. The two reflections observed under high pressure were indexed as a cubic perovskite form and each unit cell volume was calculated. The bulk modulus, K_0=183(±10) GPa, obtained by fitting with the Birch's equation. This value is consistent with the previous reported K_0 value (K_0=198 GPa) of $CaGeO_3$-perovskite (Liebermann et al., 1977). This evidence also supports that the perovskite structure appears above 15 GPa. The reflection

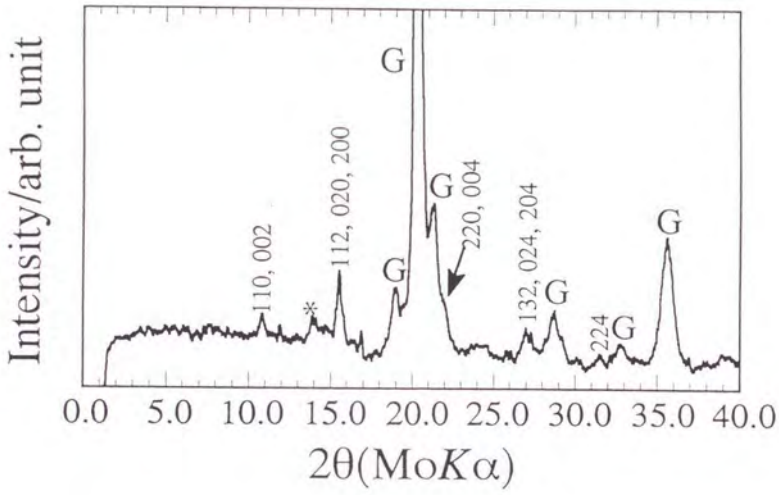

Fig. 23. X-ray diffraction pattern of a recovered sample of $CaGeO_3$ from 27 GPa which is indexed as the perovskite-form (Sasaki et al., 1983).
G represents the reflections from a gasket. * shows the reflection from the wollastonite-form.

Table 2. X-ray diffraction data of a recovered $CaGeO_3$ sample from 27 GPa.

hkl	*d* obs	*d* calc
110	3.75(5)	3.7231
002		2.6337
020	2.63(5)	2.6332
112		2.6307
200		
220	1.86(2)	1.8611
004		1.5207
132	1.52(2)	1.5203
024		1.5194
204	1.31(2)	1.3163
224		

The values of *d* calc are calculated on the basis of the perovskite-form of $CaGeO_3$ reported by Sasaki et al. (1983).
Note: a=4.832(11), b=5.031(13), c=7.022(16) Å.

corresponding to d=6.37(8) Å represents that some structural modification is taking place under high pressure. In addition, there are numerical relations of each d-value, namely, $6.37/3.65 \approx \sqrt{3}$ and $3.65/2.57 \approx \sqrt{2}$.

4.2.2 *Diffraction profiles by MAX80*

Diffraction profiles measured at about 6.8, 8.8 and 12.2 GPa with increasing temperature by using MAX80 is expected to contribute to clarify the stability of $CaGeO_3$-rhodonite appeared above 6 GPa in the present DAC experiment. Fig. 24(a), (b), (c) show the change of diffraction profiles with increasing temperature at about 6.8, 8.8 and 12.2 GPa, respectively. The two strongest peaks of $CaGeO_3$-rhodonite can be also detected remarkably in the high pressure and temperature experiments by the cubic anvil type device (MAX80).

The garnet-form appeared above about 500°C in the run at 6.8 GPa. The perovskite-form finally detected with increasing temperature both in a 8.8 GPa- and a 12.2 GPa-run. The ratio of intensity between the main reflection of the wollastonite-form and the $\bar{1}40$ reflection of the rhodonite-form, which corresponds to a longer d-value between the two strongest peaks, is presented in Fig. 25(a), (b), (c). The record number stands for the lapse of time, but does not necessarily represent a linear function of either time or temperature. Before a thermodynamically stable phase appear, the intensity of the reflection of the rhodonite-form becomes stronger in comparison with the main reflection of the wollastonite-form. This evidence indicates that $CaGeO_3$-rhodonite may be stable rather than the wollastonite-form under high pressure at moderate temperature (from room temperature to about 400°C). The intensities of the peaks of the rhodonite-form were suddenly

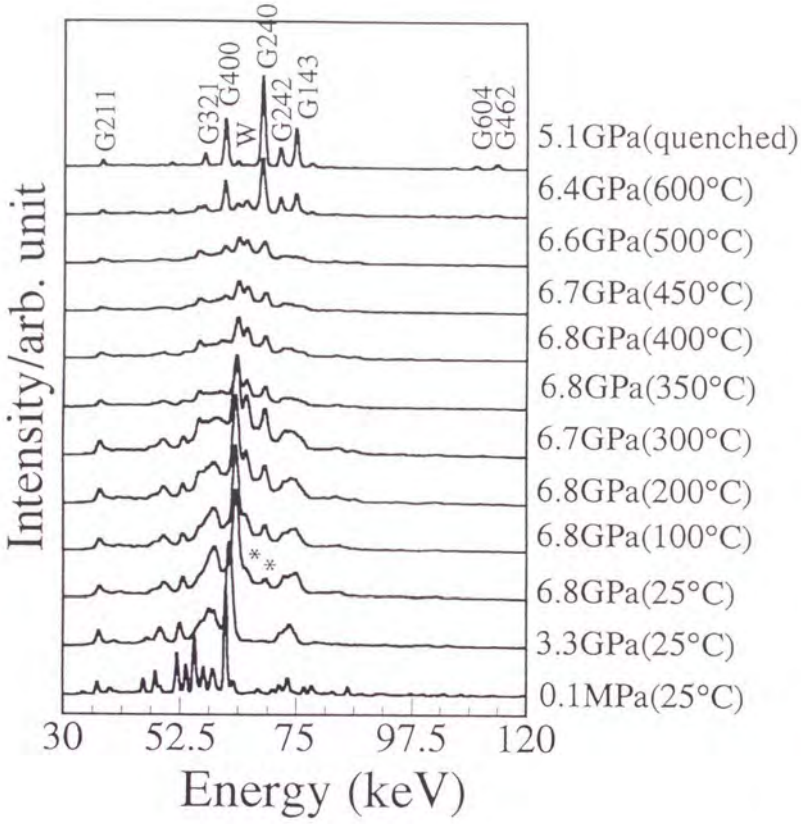

Fig. 24(a). X-ray diffraction patterns of $CaGeO_3$ at about 6.8 GPa with increasing temperature.
G*hkl*s show the reflections indexed as the garnet-form.
* represents the reflections from an intermediate phase with the rhodonite structure.
W shows the main reflection from the wollastonite-form.

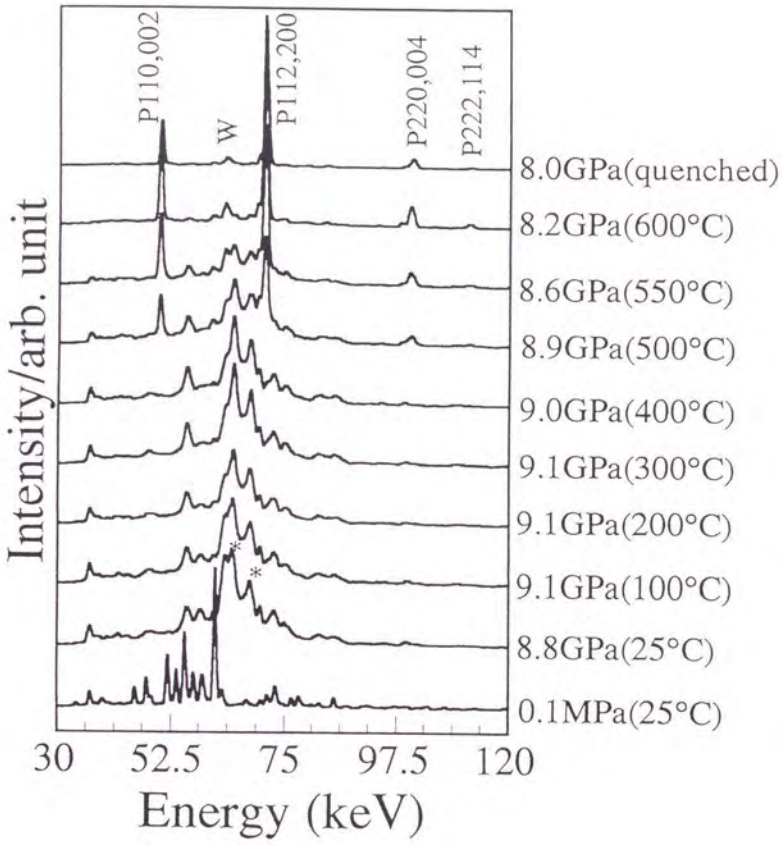

Fig. 24(b). X-ray diffraction patterns of $CaGeO_3$ at about 8.8 GPa with increasing temperature.
P*hkl*s show the reflections indexed as the perovskite-form.

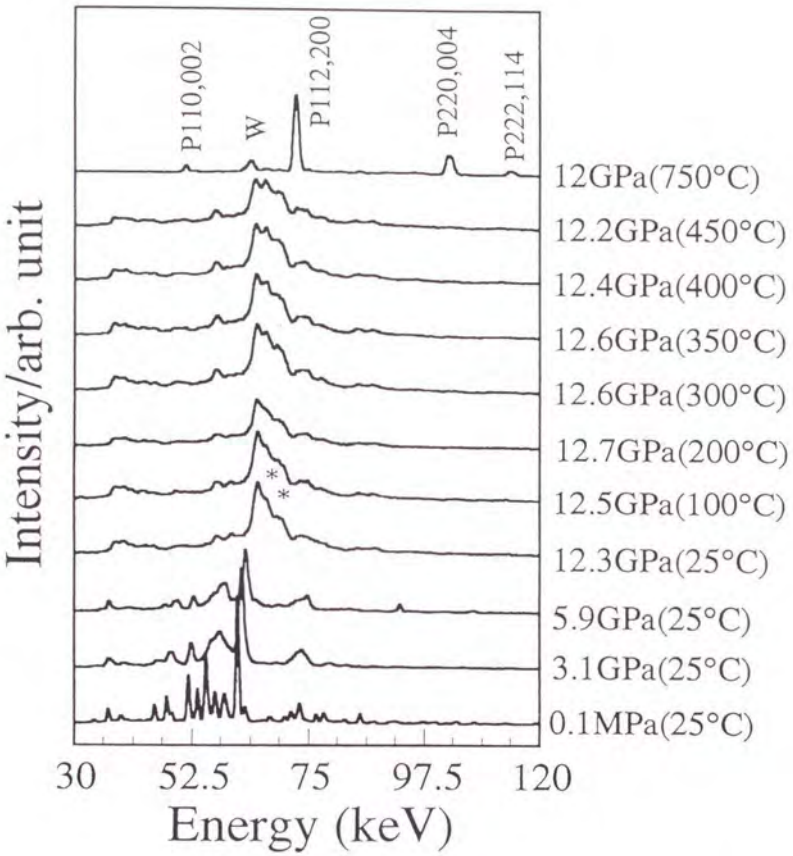

Fig. 24(c). X-ray diffraction patterns of $CaGeO_3$ at about 12.2 GPa with increasing temperature.
P*hkl*s show the reflections indexed as the perovskite-form.

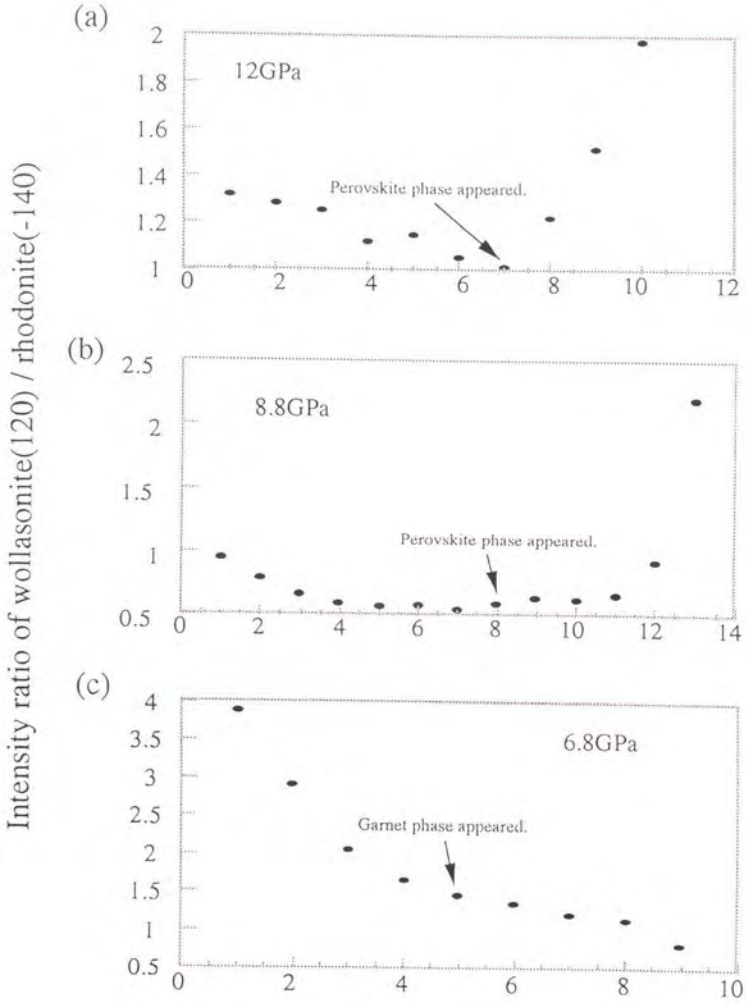

Fig. 25. Plots of the ratio of peak intensity between the main reflection of $CaGeO_3$-wollastonite and the main reflection of an intermediate phase (the rhodonite-form) *versus* the record number. The record number shows the lapse of time, however, it does not necessarily represent a linear function of either temperature or time.

(a) 12GPa, (b) 8.8GPa, (c) 6.8GPa.

weakened, when some peaks of the perovskite-form or the garnet-form can be observed. This evidence suggests that $CaGeO_3$-rhodonite is not a thermodynamically stable phase, but a "kinetically metastable" phase. $CaGeO_3$-rhodonite becomes suddenly unstable, when the perovskite-form appears rather than the garnet-form appears.

4.2.3 *Density*

The density of $CaGeO_3$-wollastonite calculated from the X-ray diffraction experiments is about 3.8 g/cm^3 under ambient conditions. Liebau (1960) reported that it is 3.79 g/cm^3. The density of the garnet-form of $CaGeO_3$ is 4.412 g/cm^3 (Prewitt and Sleight, 1969) and that of the perovskite-form of $CaGeO_3$ is 5.171 g/cm^3 (Sasaki et al., 1983). Therefore the garnet-form is about 22 % denser than the wollastonite-form and the perovskite-form is about 43 % denser than the wollastonite-form under ambient conditions.

The densities determined by using the Berman density torsion balance are presented in Table 3. Although the recovered samples from high pressure experiments were too small to measure their density precisely, these data clearly show that the densities of the recovered samples are a little denser (about 3.4 %) than that of $CaGeO_3$-wollastonite and almost constant in spite of the synthesized pressures. The calculated density of hypothetical rhodonite-form of $CaGeO_3$ is about 4 g/cm^3, and the value is in good agreement with the measured densities of the recovered samples. This result also supports the wollastonite-rhodonite transition of $CaGeO_3$.

Table 3. Summary of densities of $CaGeO_3$ samples quenched from 6, 20 and 26 GPa.

Run No. Pressure	1	2	3	4	5	Average
6 GPa	3.95(6)	3.95(3)	3.97(6)	4.03(2)	4.01(5)	3.98(5)
20 GPa	3.94(5)	3.92(4)	3.86(9)	3.96(2)	3.98(5)	3.93(4)
26 GPa	3.88(3)	3.99(9)	3.87(3)	3.83(1)	4.01(8)	3.92(3)

4.3 $MgGeO_3$

Diffraction profiles of $MgGeO_3$ obtained by *in-situ* X-ray diffraction measurements using the DAC up to 35 GPa at room temperature (Fig. 26) show that the profiles up to 16.4 GPa are essentially the same as that of the starting materials. The cell dimensions up to 16 GPa determined by a least-squares method using about 12 observed reflections are plotted in Fig. 27(a),(b). The cell edges decrease almost linearly with pressure. It seems that the direction of a-axis is a little more compressed than that of other axes. The β angle becomes smaller with increasing pressure. Calculated volume data were fitted with the Birch's equation of state. The ratios of V/V_0 with increasing pressure are represented in Fig. 28. The K_0 value presently obtained is,

$$K_0=127(\pm 8)\ \text{GPa}$$

, which is consistent with the previously reported value $K_0=131$ GPa (Liebermann, 1974) obtained by means of measurements of elastic wave velocity under pressure. This agreement indicates that the present data provide a reliable measure of the bulk modulus of $MgGeO_3$-high-clinoenstatite.

The result of *in-situ* X-ray diffraction measurements shows that no drastic change takes place up to 23 GPa. No extra reflection appears except for diffraction peaks diffracted from the $MgGeO_3$-high-clinoenstatite. Diffraction peaks start broadening gradually above 10 GPa. The broadening of diffraction profile makes unclear the separation of each peak and some diffraction peaks are diminished and disappeared with increasing pressure. It is a possible interpretation that the effect of non-hydrostatic pressure causes the profile broadening. However, the deviation from hydrostatic condition seems to be small at around 10 GPa, even if the pressure medium consisting of the 4:1 mixture of methanol and ethanol is transformed into a glass state at pressure

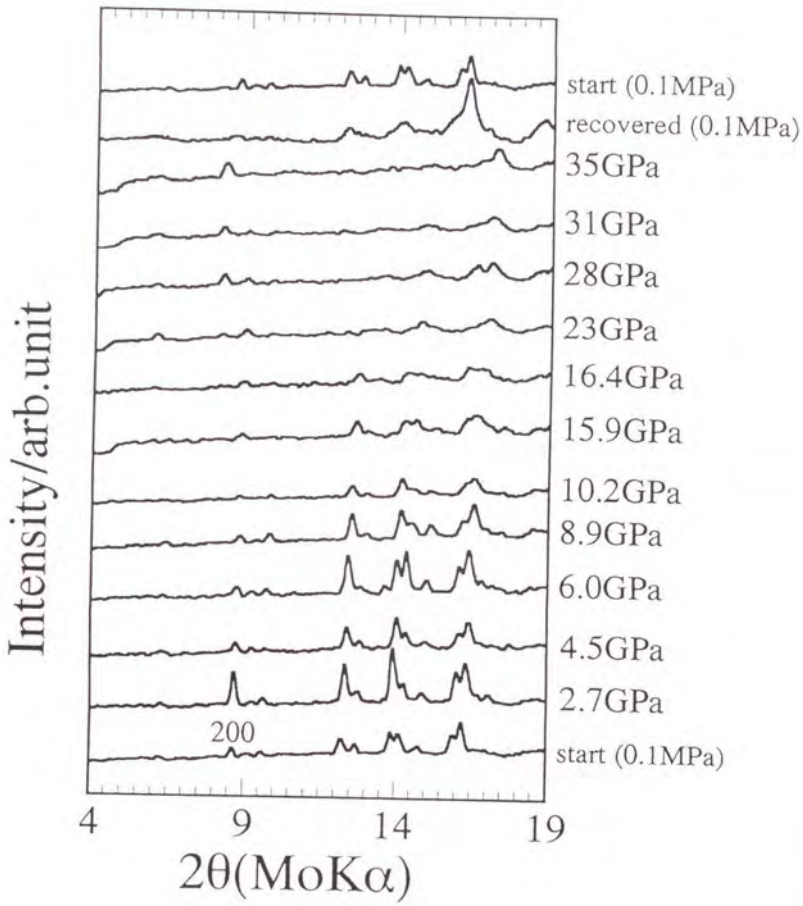

Fig. 26. X-ray diffraction patterns of $MgGeO_3$-high-clinoenstatite on compression up to 35 GPa.

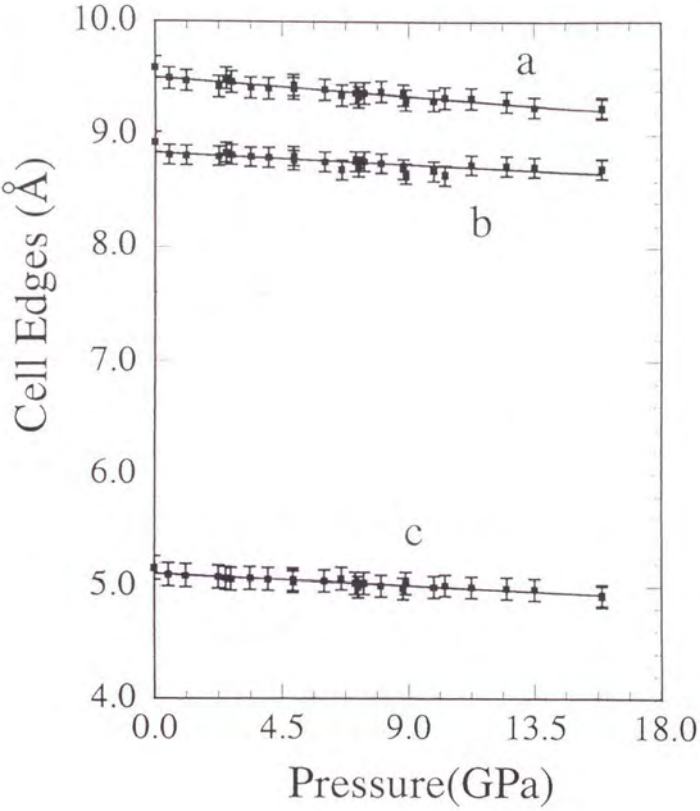

Fig. 27(a). Plots of cell dimensions (a, b, c) *versus* pressures of $MgGeO_3$-high-clinoenstatite.

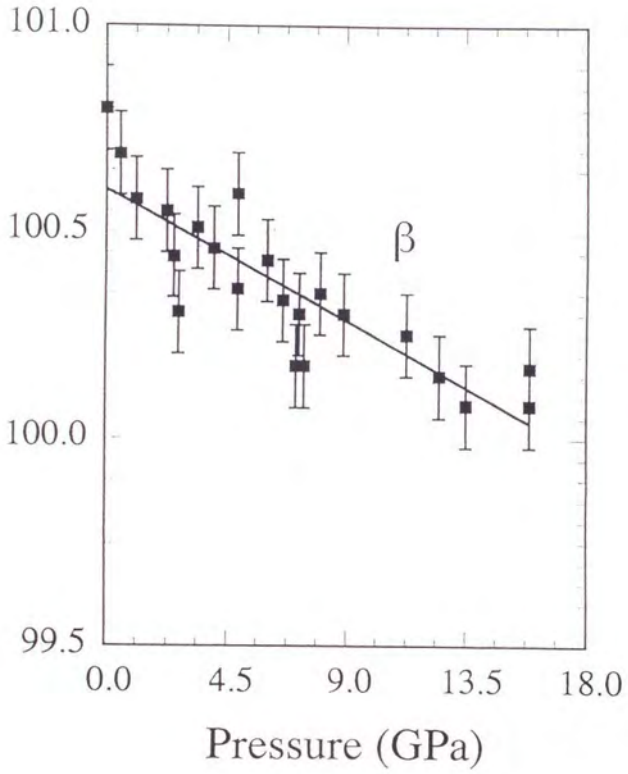

Fig. 27(b). Plots of β angle (°) *versus* pressures of $MgGeO_3$-high-clinoenstatite.

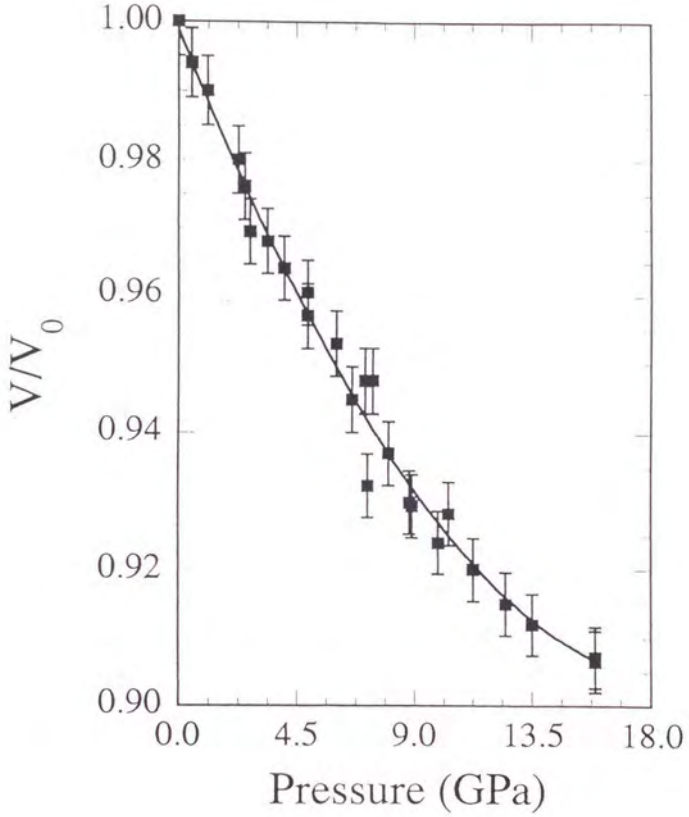

Fig. 28. Variation of V/V_0 with increasing pressure on $MgGeO_3$-high-clinoenstatite. A solid curve fitted by the Birch's equation of state.

above 11.1 GPa (Piermarini et al., 1973). Indeed, the pressure distribution in the gasket hole was within 0.5~1.0 GPa at 15 GPa. Therefore, it is concluded that some structural modification starts occurring at about 10 GPa.

The subsequent change of diffraction patterns occurs from about 23 GPa. Three new peaks appear in diffraction patterns. With increasing pressure, the peak of 2θ=6.02(8)° at 23 GPa decreases in its intensity. On the other hand, each profile of the other two peaks becomes clearer. And only two peaks with 2θ=8.21(7)° and 17.16(5)° in the diffraction pattern at 35 GPa can be apparently detected. The diffraction patterns of the $MgGeO_3$-high-clinoenstatite and a recovered sample from 35 GPa shown in Fig. 29 indicated that the new observed transition is reversible, although the broadening of each profiles takes place.

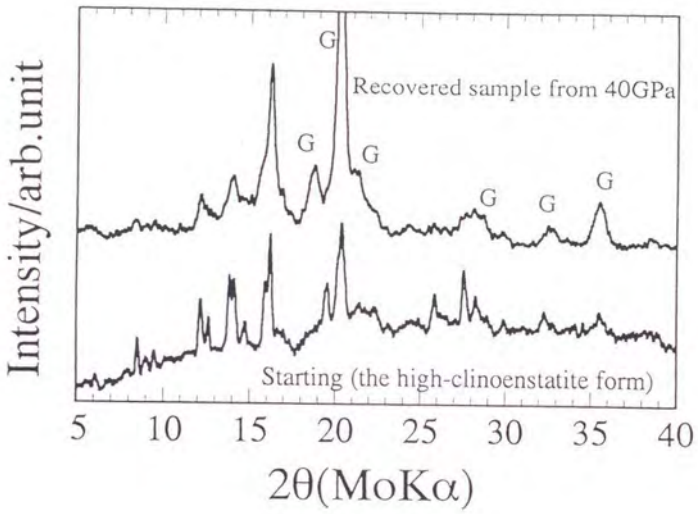

Fig. 29. X-ray diffraction patterns of a recovered sample from 40 GPa and a starting sample of $MgGeO_3$-high-clinoenstatite.
G represents the reflections from a gasket.

4.4 Mg_2GeO_4

Diffraction patterns of Mg_2GeO_4-olivine obtained by *in-situ* X-ray diffraction measurements using a DAC in compression process up to 35 GPa and in decompression process to ambient pressure at room temperature (Fig. 30), show that the diffraction patterns up to 15.1 GPa are essentially the same as that of the starting materials. The cell dimensions up to 15 GPa were determined by a least-squares method using about 10 observed reflections, which are plotted versus pressures in Fig. 31. The change of the V/V_0 ratio with increasing pressure is shown in Fig. 32. The cell dimensions show the almost linear dependence on the pressure and no remarkable crick is observed. This evidence suggests that a drastic structural change never occurred up to about 15 GPa. Calculated cell volume data were fitted with the Birch's equation of state and the obtained K_0 value is

$$K_0=70(\pm5)\ \text{GPa}.$$

This value is consistent with the previously reported the value of K_0=74.6 GPa (Will and Lauterjung, 1992). This consistency indicates that the present X-ray measurements provide a reliable value of the bulk modulus of Mg_2GeO_4-olivine.

Between 15.1 GPa and 22.7 GPa, all diffracted X-ray peaks of Mg_2GeO_4-olivine become weaker and some diffraction peaks disappear. Only 021 reflection, which is a main peak of Mg_2GeO_4-olivine, can be observed at 25.3 GPa, but no diffraction peak can be detected except a diffraction line from solid argon at 30.1 GPa, suggesting the amorphization of the sample. The Ge fluorescence in addition to the reflection from the solid argon were detected in the diffraction pattern. Argon used as a pressure medium is transformed into a solid state at pressure above 1 GPa. The diffraction peak from solid argon

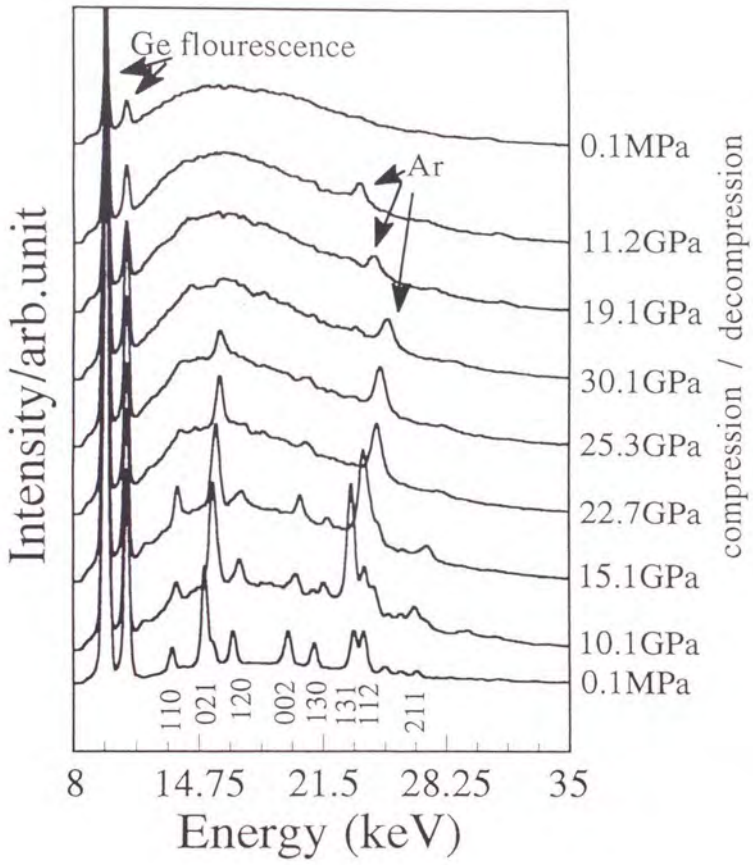

Fig. 30. X-ray diffraction patterns of Mg_2GeO_4-olivine on compression and on decompression.

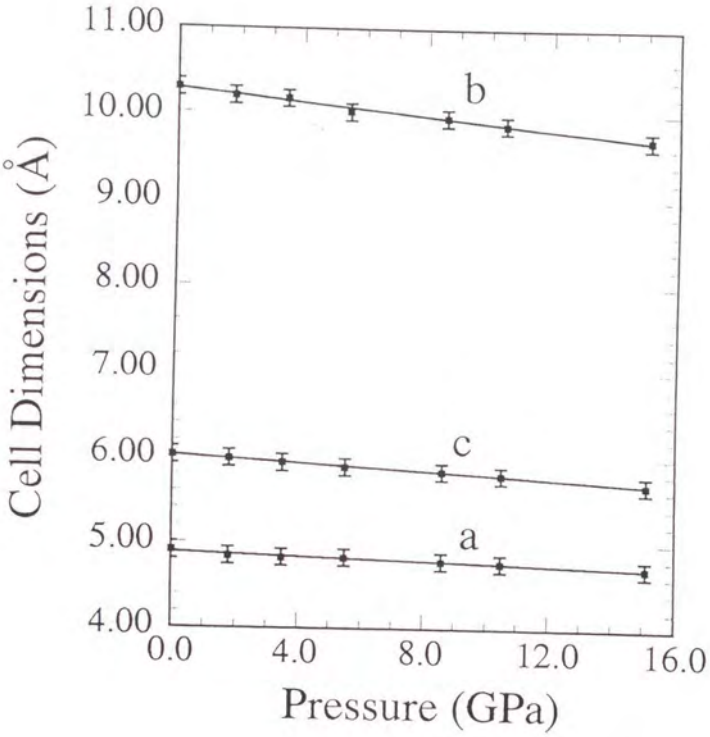

Fig. 31. Diagrams of cell dimensions *versus* pressures of Mg_2GeO_4.

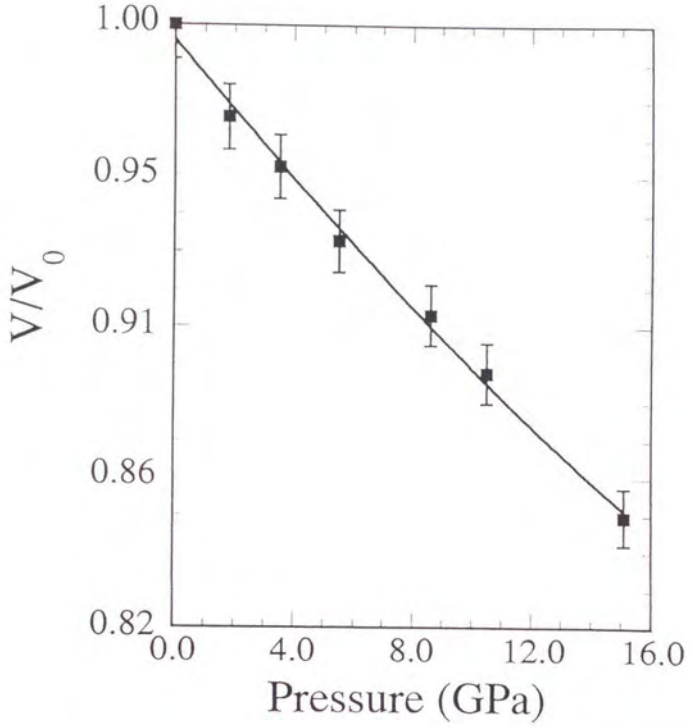

Fig. 32. Variation of V/V_0 with increasing pressure on Mg_2GeO_4-olivine. A solid curve fitted by the Birch's equation of state.

disappears under decompression to ambient pressure, because argon is a gas state under ambient conditions.

Any unidentified diffraction peaks did not appear from 0.1 MPa to 35 GPa. And no peak also appears in the diffraction pattern in decompression process, even at ambient pressure. The fact that all diffraction peaks of Mg_2GeO_4-olivine disappear at about 30 GPa, indicates that Mg_2GeO_4-olivine is transformed to an amorphous state for the X-ray diffraction at about 30 GPa and that its transformation is irreversible.

5. Discussion

5.1 $CaGeO_3$

5.1.1 *Compression mechanism of $CaGeO_3$-wollastonite*

Andrault et al. (1992) calculated the bulk modulus of the GeO_4 tetrahedron in $CaGeO_3$-wollastonite on the basis of their XAFS data:

$$K[GeO_4] \geq 280 \text{ GPa}$$

This value is remarkably different from the value of the bulk modulus of $CaGeO_3$-wollastonite. Hazen and Prewitt (1977) and Hazen and Finger (1979) proposed the relationship between bond strength and compressibility of individual cation coordination polyhedra as:

$$\{\text{compressibility}\} \propto \{\text{polyhedral volume}\} / \{\text{cation charge}\}.$$

The compressibility is a reciprocal number of the bulk modulus. This means that the CaO_6 octahedron is compressed much more than the GeO_4 tetrahedron. The value of the bulk modulus of the CaO_6 octahedron has been estimated to 85 GPa in a *C*2/*c*-pyroxene ($(Ca_{0.87}, Mg_{0.59}, Fe^{2+}_{0.21}, Ti^{4+}_{0.06}, Al_{0.17})(Si_{1.72}, Al_{0.28})O_6$-fassaite)) by the single crystal X-ray diffraction study under high pressure (Hazen and Finger, 1977). This value is much smaller than that of the GeO_4 tetrahedron (≥280 GPa) and is comparable to that of $CaGeO_3$-wollastonite. Therefore, the GeO_4 tetrahedron is very rigid and the compression mechanism in $CaGeO_3$-wollastonite seems to be controlled by the compression of the CaO_6 octahedra up to 6 GPa.

5.1.2 *Wollastonite-rhodonite transition*

The metastable wollastonite-rhodonite transition has been confirmed under high pressure at kinetically low temperature by the *in-situ* experiments. $CaGeO_3$-wollastonite belongs to the pyroxenoid group, in which the structures

have one dimensional single chains consisting of the GeO_4 tetrahedra (Fig. 2).

It is well known that the number of repeat units of the SiO_4 (or GeO_4) tetrahedron in the chain of pyroxenoid and pyroxene increases with decreasing the average size of the octahedral cations. It is also known that the number of tetrahedral repetition in the pyroxenoids' chain increases under high pressure. For example, Akimoto and Syono (1972) found that the rhodonite-form of $MnSiO_3$ transforms firstly to the pyroxmangite-form and then to the clinopyroxene-form. The number of repeat units in their chains is five, seven and infinite, respectively.

The crystal structures of pyroxenoids and pyroxenes are built up by approximately cubic close packed oxygen atoms. The pyroxenoids-to-pyroxene transition is capable under high pressure, since the arrangement of oxygen atoms becomes more closed packing.

The compression mechanism of $CaGeO_3$-wollastonite controlled by the compression of the CaO_6 octahedra induce the change of the repetition of the chain unit, resulting in the same effect, as the average size of the octahedral cation decreases. Therefore it is reasonable that $CaGeO_3$-wollastonite is transformed into the rhodonite-form under high pressure.

5.1.3 *Transition to $CaGeO_3$- perovskite*

It is confirmed that $CaGeO_3$-perovskite appears above 15 GPa in this study. And the samples synthesized under high pressure by a multianvil apparatus include an amorphous phase . $CaGeO_3$-perovskite is well known as a quenchable phase under ambient conditions (Sasaki et al., 1983). In the case of α-quartz of GeO_2, an oxygen coordination change from fourfold to sixfold occurs during a pressure-induced amorphization (Itie et al., 1989). Wolf et al.

(1992) found that the X-ray amorphous state is a mixed phase which consists of extremely small crystallites of the α-quartz-form and the rutile-form, which is a high pressure phase of the α-quartz-form. The increase in the ratio of the rutile-form to the α-quartz-form with pressures, is supported by the evidence that a recovered sample from a higher pressure is denser than samples synthesized at a lower pressure (Yamanaka et al., 1992). In the case of $CaGeO_3$, however, the result of density measurements of recovered samples indicates that the densities are almost constant regardless of the synthesized pressure. This evidence suggests that the recovered samples of $CaGeO_3$ may not include perovskite nuclei at ambient pressure.

Andrault et al. (1992) observed *in-situ* XAFS signals of $CaGeO_3$-wollastonite up to 23 GPa by using a DAC. According to their data, the Ge-O distance is almost constant at about 1.76 Å up to about 7 GPa, because GeO_4 tetrahedron is very rigid. And the distance gradually increases from 7 GPa to about 15 GPa, and then becomes almost constant above 15 GPa. Andrault et al. (1992) concluded that the coordination change of Ge atoms occurred from fourfold to sixfold under high pressure.

The onset pressure, at which some change occurs, is comparable between the present diffraction data and the XAFS data. The transition from $CaGeO_3$-wollastonite to the rhodonite structure which is confirmed in this study, however, does not accompany the coordination change of constituent atoms. On the other hand, $CaGeO_3$-perovskite has sixfolded Ge atoms. Therefore, it is suggested that the coordination change is related to the transition from the rhodonite-form to the perovskite-form.

The XAFS data (Andrault et al., 1992) also suggested that almost all the Ge atoms in a recovered sample have four-fold coordination. This reversible

change of the coordination number also supports that the amorphous phase in the recovered samples may not include perovskite nuclei at ambient pressure.

The 101 plane of the wollastonite-form represents a stacking plane which is parallel to close-packed oxygen layers and the intensity of the 101 reflection is maintained up to 20 GPa. The persistent existence of the 101 reflection indicates that the structural framework of the close-packed oxygen atoms may be basically preserved even in the amorphous phase. Then, the XAFS data can be interpreted as Ge atoms in the tetrahedral site move to their adjacent octahedral site locally at high pressures.

5.2 $MgGeO_3$

5.2.1 *Compression mechanism of $MgGeO_3$-high-clinoenstatite*

Andrault et al. (1992) calculated the value of the bulk modulus of the GeO_4 tetrahedron in $MgGeO_3$-high-clinoenstatite by XAFS data:

$$K[GeO_4]_{MgGeO_3} \sim 135 \text{ GPa}$$

The value of the bulk modulus of the GeO_4 tetrahedron in $MgGeO_3$-high-clinoenstatite is similar to that of the MgO_6 octahedron in forsterite, $K[MgO_6]_{forsterite}$=150 GPa (Hazen, 1976) and the bulk modulus of $MgGeO_3$-high-clinoenstatite (K_0=127(±8) GPa). This relation is different from the case of $CaGeO_3$-wollastonite, and such a relation suggests that the compression of $MgGeO_3$-high-clinoenstatite is due to homogeneous polyhedra compression.

It is known that the arrangement of oxygen atoms in $MgGeO_3$-high-clinoenstatite with space group *C2/c* is almost ideal cubic close packing (CCP) under ambient conditions (Yamanaka et al.,1985). It is probable that the arrangement of the oxygen packing approaches to more ideal CCP as the pressure increases. The homogeneous compression of polyhedra with

increasing pressures, as mentioned above, supports this compression mechanism. To approach to ideal oxygen packing under high pressures is quite reasonable in comparison with the result of single crystal diffraction experiment under high pressure on fassite, which is one of clinopyroxene with space group *C2/c* (Hazen and Finger, 1977).

5.2.2 *Transition to an unidentified phase*

Only two or three reflections observed in the range from above 23 GPa, suggest that the structure appeared above 23 GPa , may have a high symmetry. Those reflections can be indexed as none of the ilmenite phase, the $LiNbO_3$ phase and the perovskite phase, which are high pressure polymorphs of $MgGeO_3$-high-clinoenstatite. Both the ilmenite phase and the $LiNbO_3$ phase are quenchable. Although the perovskite phase is stabilized only at high pressure, the perovskite phase would be recovered as the $LiNbO_3$ phase under ambient conditions (Leinenweber et al., 1994). However, the X-ray diffraction profile observed above 23 GPa in this study is not maintained at ambient pressure and is indexed as $MgGeO_3$-high-clinoenstatite. These evidences indicate that the unidentified phase may not correspond to the ilmenite-form, the $LiNbO_3$ form or the perovskite-form. Because it is probable that some thermodynamically metastable phase allows to appear in the process of metastable compression, the new phase may be a new kinetically metastable phase.

Andrault et al. (1992) performed that *in-situ* XAFS measurements of $MgGeO_3$-high-clinoenstatite under high pressure and the Ge-O distances were calculated. The Ge-O distance of $MgGeO_3$ decreases up to 8.5 GPa and then gradually increases up to about 21 GPa. They concluded that the increase of the Ge-O distance may correspond to a pressure-induced coordination change of the

Ge atom from four-fold to six-fold.

The Ge-O distances calculated from the XAFS data represents as the average Ge-O distance in the bulk sample. The Ge-O distances become longer with increase of the mixing ratio of the α-quartz-form and the rutile-form in the case of GeO_2. The onset pressure, at which some modification takes place in the present diffraction data, seems to be consistent with the XAFS data. The consistency suggests that some structural modification at about 10 GPa is related to the partial coordination change of Ge atoms from four-fold to six-fold. Accordingly, the calculated Ge-O distances in $MgGeO_3$ may indicate that the transition to the unidentified phase start at about 10 GPa and that there is a mixed region of $MgGeO_3$-high-clinoenstatite and the unidentified phase from the pressure of 8.5 GPa to 21 GPa. The size of crystallites of the unidentified phase below 23 GPa may be so small as incoherent to the X-ray wave length, and the crystallites grow into a large enough to be coherent to the X-ray wave length used. The unidentified phase may have partly six-fold coordinated Ge atoms, which is metastable under ambient conditions.

5.3 Mg_2GeO_4

5.3.1 *Compression mechanism of Mg_2GeO_4-olivine*

The bulk modulus of the MgO_6 octahedron in forsterite, $K[MgO_6]_{forsterite}$=160 GPa, reported by Hazen (1976) is much larger than that of Mg_2GeO_4-olivine (K_0=70 GPa). The bulk modulus of the GeO_4 tetrahedron in Mg_2GeO_4-olivine should be also larger than that of the MgO_6 octahedron, according to the relation among compressibility, polyhedral volume and cation charge. Such an extraordinary small value of the bulk modulus of Mg_2GeO_4-olivine, therefore, suggests that compression may be due to a combination of

metal-oxygen and oxygen-oxygen compression.

If the oxygen atoms of the olivine structure is arranged in an ideal manner of HCP with the a-axis perpendicular to the oxygen layers, the cell volume of olivine structure, V_{HCP}, can be given by the following equation.

$$V_{HCP}=3\sqrt{3}a^3/2$$

From the fact that the ratio between the observed cell volume, V_{Obs}, and V_{HCP} in Fig. 33 is almost unity up to 4 GPa, we expect that the arrangement of the oxygen atoms of the olivine structure constitute an ideal HCP. Structural distortion from HCP seems to start occurring above 4 GPa (Fig. 33).

Guyot and Reynard (1992) suggested that Mg_2SiO_4-forsterite undergoes a crystal-to-amorphous transition above 70 GPa and they also showed by a transmission electron microscopy (TEM) study that its intermediate phase which has an ideal close-packed oxygen sublattice and a glassy cation sublattice of recovered samples from high pressure. And they claimed that the structure was related to an intermediate phase which was observed in the process of the olivine-spinel transition (Will and Lauterjung, 1987, Furnish and Bassett, 1983). Reynard et al. (1994) proposed that pressure-induced structural modifications associated with the transition from olivine to hypothetical ω- or ε*-phase takes place between 11 GPa and 22 GPa on the basis of their *in-situ* Raman spectroscopic study. The ω- or the ε*-phase is structurally close to a disordered spinelloid proposed by Hyde et al. (1982) and Madon and Poirier (1983). The pressure, at which some modifications are observed in the Raman signals, seem to be consistent with the pressure where some reflections start disappearing in presently obtained diffraction patterns. However, there is no evidence to support the transition to some spinelloid structure in the diffraction profiles under high pressure.

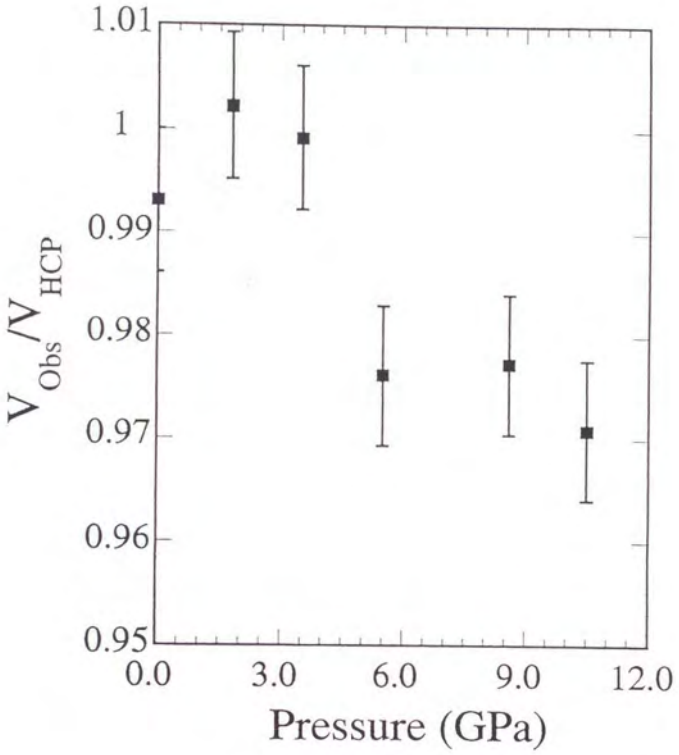

Fig. 33. A plot of the ratio of observed cell volume (V_{Obs}) to calculated cell volume (V_{HCP}) *versus* pressures.

5.3.2 *Amorphization*

Mg_2GeO_4-olivine is transformed into amorphous phase above 30 GPa. No structural information is presently available on "X-ray amorphous Mg_2GeO_4". It is one of possible interpretations that a gradual decrease in the crystallite size of the high pressure form results in "X-ray amorphous" state. When the crystalline substance is subjected to mechanical crushing up to the extremely fine particle incoherent to the X-ray wave length used, it becomes X-ray amorphous state. If grains are crashed mechanically, it is hard to consider that the coordination change of cation occur. It is believed that argon pressure medium keeps good hydrostatic state up to fairly high pressure, even if argon is transformed into a solid state at pressure above 1 GPa (McMahan, 1986). The deviation from hydrostatic state is not likely to lead to mechanical crashing of grains below pressure of 30 GPa. Therefore, the author concludes that the pressure-induced amorphization in the case of Mg_2GeO_4-olivine is not an experimental problem but a substantial crystal-to-amorphous transition.

Williams et al. (1990) reported that Fe_2SiO_4-fayalite undergoes a pressure-induced amorphization and that the long-rang order is not recovered upon decompression on the basis of the analysis of infrared spectra. They also suggested that the high-pressure amorphization may be associated with the pressure-induced coordination change of silicon atoms in Fe_2SiO_4 from four-fold to six-fold.

Reynard et al. (1994) observed the Raman vibrational bands of either polymerized GeO_4 tetrahedra or of six-fold coordinated Ge atoms in the Raman spectrum of the sample of Mg_2GeO_4-olivine quenched from 34.4 GPa. They suggested that some structural changes took place in Mg_2GeO_4 above 30 GPa. In addition the result of *in-situ* infrared spectroscopic measurement under

pressure for Fe_2SiO_4 (William et al., 1990) and the molecular dymanics (MD) calculation for forsterite (Dejima,1994) indicated that the coordination change of Si atoms may cause the pressure-induced amorphization. In this case, high pressure amorphous state must be an intermediate state in a transition process of olivine to some phase having six-folded Ge or Si atoms.

It has never been reported that the chemical composition of Mg_2GeO_4 has no stable polymorph having six-folded Ge atoms. After decomposition into the $MgGeO_3$ polymorph and rock salt (MgO), six-fold coordinated Ge atoms appear in the $MgGeO_3$ polymorph. It is unclear that the phase having six-fold coordinated Ge or Si atoms may be $MgGeO_3$ polymorphs or some other phases. Only MD calculation predicted a phase having six-folded Si atoms without decomposition (Dejima, 1994). According to the calculation, the new high pressure phase of forsterite has six-fold coordinated Si atoms and is composed of the close-packed oxygen atoms (stacking sequence ABA'B').

5.4 *General discussion*

5.4.1 *Mechanism of a pressure-induced amorphization*

Logic. When all the X-ray diffraction peaks of a low pressure phase disappeared under high pressure, we judge that the pressure-induced amorphization takes place. However, the experimental data on $CaGeO_3$ and $MgGeO_3$ confirm that the X-ray amorphous state, which is observed under high pressure at kinetically low temperature, is the mixed compounds composed of extremely fine crystallites of a low pressure and its high pressure phase.

The amorphization is considered as a kinetically hindered phenomenon during the transition to a high pressure phase. Generally, the pressure-induced phase transition at room temperature is more sluggish than the thermal-induced

transition, because of the small increments of activation energy. It is suggested that the pressure-induced transition continues in the wide range of pressure at room temperature. Therefore, the balance of the following two factors determines the occurrence of the X-ray amorphous state. One factor is the conversion rate of the structural transition initiated by the modification of the local structure in a low pressure phase and the other is the nucleation-and-growth rate of a high pressure phase. Accordingly, when the structure of a low pressure phase is distorted severely and the long range order vanishes before the crystallites of its high pressure phase grow above the coherent size to X-ray wave length used, no reflections in the X-ray diffraction pattern could be detected. On the other hand, when a high pressure phase can be observed before all X-ray diffraction peaks of a low pressure phase disappear, the X-ray amorphous state can not be observed. The former case applies to Mg_2GeO_4 and the case of $CaGeO_3$ and $MgGeO_3$ are examples of the latter case. If the transition is accompanied with the coordination change, the sign of the transition may appear in the XAFS data and in the Raman spectra without changing the diffraction profile.

Generally, there is a critical size of nuclei in the nucleation process. If nuclei are smaller than the critical size, the nuclei will be dissolved and disappear because the increment of the surface energy with the nucleation of a high pressure phase, increases the total free energy in the system. And if the size of nuclei becomes larger than that of the critical nuclei, the nuclei will continue to grow, because the reduction of the volume energy accompanied by the transition to a high pressure phase, compensates the increment of the surface energy. The critical size of nuclei depends both on the materials and on the p-T conditions. This consideration suggest that the nuclei of a high pressure phase

are not necessarily stable under ambient conditions, even if there are nuclei under high pressure. The relation between the critical nuclei and the coherent size of crystallite to X-ray wave length is unclear and may depend on the material.

The pressure-induced amorphization of the three germanates will be explained as follows on the basis of this interpretation.

Modification of the crystal structures. The modification of the crystal structures under high pressure at kinetically low temperature probably relates to the stacking sequence of oxygen atoms in the three germanates. Noted that the arrangement of oxygen atoms is Cubic Closed Packing (CCP) for $CaGeO_3$-rhodonite and $MgGeO_3$-high-clinoenstatite, and is Hexagonal Closed Packing (HCP) for Mg_2GeO_4-olivine.

Generally, Ge atoms tend to prefer six-fold to four-fold coordination under high pressure. Indeed, the XAFS data (Andrault et al., 1992) and the Raman data (Reynard et al., 1994) on $CaGeO_3$, $MgGeO_3$ and Mg_2GeO_4, indicated that a Ge atom is coordinated with 6 oxygen atoms under high pressure. The results in this study suggest that the structural modification under high pressure begins with the movement of Ge atoms to the octahedral site locally without breaking the structural framework composed of oxygen packing, as discussed in 5.1.3, 5.2.2 and 5.3.2.

If the Ge atoms are locally sit on the octahedral sites in the olivine structure, many face-sheared octahedra are formed (Fig. 6). The Pauling's third rule (1929) argued that face-shearing of polyhedron is unstable, because of the electrostatic cation-cation repulsion. The structural framework composed of the HCP oxygen atoms, is not suitable for accommodating many six-fold coordinated cation, because such a structure contains face-shared

octahedra. Oxygen atoms in the corundum and the ilmenite structure are arranged in HCP and cations are located at its octahedral interstices, resulting in face-sheared octahedra. Such an arrangement is expected to be unstable crystal structures. However, there are exceptions on the basis of the modified Pauling's third rule by Baur (1972): Ionic structures with shared polyhedral faces can only be stable, if their geometry allows the shortening of the shared polyhedral edges. This shortening makes the cation-cation spacing longer. The octahedral cations are moved toward the vacant sites. Cation distribution in the corundum and the ilmenite structure is such a case. It is impossible to realize such geometrical constraints of cation distribution in Mg_2GeO_4 as described above. Therefore, the electrostatic instability accompanied by the local change of the Ge coordination in Mg_2GeO_4-olivine promotes the collapse of the crystal structure. Thus, the instability is related to both geometry of oxygen packing and cation distribution.

In contrast, the octahedral sites in the CCP oxygen arrangement have no shared-face . Such kind of instability as mentioned above, are not realized for the pyroxene and the pyroxenoid structures, in which the oxygen atoms are namely arranged in the manner of the CCP. The mechanism of Si migration proposed by Aikawa (1979) may apply to the coordination change of the Ge atom. A Ge atom moves from a tetrahedral site to another tetrahedral site through an adjacent vacant octahedral site in the process of the transition within the pyroxenoid group. A Ge atom in octahedral site in the course of the migration is relatively stable. Therefore the Ge atoms may settle metastably in initially vacant octahedral site at kinetically low temperature. This mechanism may be consistent with the diffraction data in this study, because Ge atoms move within the layers of CCP oxygen atoms in this process. Consequently, the X-ray

diffraction peak representing the stacking sequence which is parallel to close-packed oxygen layers is preserved up to quite high pressure.

If part of Ge atoms move to the octahedral sites and seat at the sites in $CaGeO_3$-rhodonite and $MgGeO_3$-high-clinoenstatite, the local structural modification seems to have a little influence on their surroundings. Therefore, the structural distortion of the rhodonite-form and the high-clinoenstatite-form is very sluggish and it is expected that X-ray diffractions persists at considerably high pressure.

Nucleation and growth. The present results show $CaGeO_3$-wollastonite approaches to the perovskite-form with increasing pressure through the kinetically metastable phase of the rhodonite-form. It is believed that there are nuclei of the perovskite-form below the pressure of 15 GPa, even if the reflections of the perovskite-form are observed only above 15 GPa in the X-ray diffraction pattern. This is supported by the change of the Ge-O distance calculated by XAFS data. The fact that the densities of recovered samples are almost constant regardless of the synthesized pressure, can be explained by a hypothesis that the nuclei of the perovskite-form are smaller than the critical size to be stabilized under ambient pressure. Then the nuclei disappear at ambient pressure. The experiment indicated that the nuclei reached the critical size at 27 GPa and the perovskite-form can be quenched up to ambient pressure.

The oxygen atoms in the perovskite structure basically arranged in the manner of the CCP. From the view point of the arrangement of oxygen atoms, it is considered that the perovskite structure is topologically similar to the structure of the pyroxenoid group. Pyroxene and the pyroxenoid group are transformed into the perovskite-form without a large scale reconstruction of oxygen framework. Such crystallographical matching probably promotes the

growth of the perovskite-form.

In the case of $MgGeO_3$, the nucleation and growth of an unidentified phase takes place above about 10 GPa, and the nuclei size becomes a coherent to X-ray wave length at 23 GPa. However, the size is smaller than the critical nuclei of the unidentified phase under ambient pressure. Therefore, the unidentified phase reverts to the high-clinoenstatite-form, because the nuclei is unstable at ambient pressure. This reversible transition suggests that the structure of the high pressure phase is topologically similar to the high-clinoenstatite and that the transition needs only a small atomic displacement.

The pressure-induced amorphization is a precursor phenomenon of the transition to a high pressure phase. Reynard et al. (1994) suggested that the coordination change of Ge atoms occurs during the amorphization. The spinel-form of Mg_2GeO_4, which is high pressure stable form of the olivine-form, does not have six-fold coordinated Ge atoms. After the decomposition into a $MgGeO_3$-polymorph and rock salt (MgO), six-fold coordinated Ge atoms appear in the $MgGeO_3$-polymorph. However, it is unlikely that such decomposition takes place at room temperature. The decomposition must require high thermal energy, because a large scale atomic motion is necessary to break the olivine structure and to recrystallize the $MgGeO_3$-polymorph and MgO. Therefore, it is hard to promote the nucleation and growth of a high pressure phase in the case of Mg_2GeO_4.

As mentioned above, the collapse of the Mg_2GeO_4-olivine structure takes place catastrophically and the nucleation and growth is difficult at room temperature. Therefore, the X-ray amorphous state is observed in Mg_2GeO_4-olivine as shown in the present *in-situ* X-ray diffraction study. On the other hand, $CaGeO_3$-rhodonite and $MgGeO_3$-high-clinoenstatite persist at a

considerably high pressure and the nuclei of their high pressure phases can grow to the coherent size to the X-ray wave length without the large thermal energy, because the local change of Ge coordination does not cause the serious instability and there is the crystallographic similarity between the low pressure phase and their high pressure phase. Therefore, it is concluded that the X-ray amorphous state has never been observed in $CaGeO_3$-rhodonite and $MgGeO_3$-high-clinoenstatite.

5.4.2 *Comparison with silicates*

Germanates have been used as analogous minerals of silicates. $CaGeO_3$, $MgGeO_3$ and Mg_2GeO_4 are analogous minerals of $CaSiO_3$, $MgSiO_3$ and Mg_2SiO_4, respectively, which are important mantle minerals. It is important to discuss the similarity and the difference between germanates and silicates of the behavior under high pressure at kinetically low temperature.

The coordination number of Ge atoms can be determined directly by the XAFS technique under high pressure in germanates. Such study made clear that a pressure-induced coordination change plays an important role on a pressure-induced structural modification and amorphization. Because of the technical problems, there remains a few unclear information about the coordination change of Si atoms under high pressure. The coordination numbers of Si atoms has been estimated by Raman experiments under high pressure (*e.g.* Reynard et al., 1994). They are not certain whether a coordination change of Si atoms occurs under high pressure and at room temperature. This study suggests that the packing model of the rigid spheres can apply to the understanding of the structural behavior under the high pressure and room temperature condition. Therefore, the coordination change of Si and/or Ge atoms under high pressure

is an important compression mechanism in both germanates and silicates.

High pressure experiments at room temperature has been performed on $CaSiO_3$-wollastonite and Mg_2SiO_4-olivine (Serghiou and Hammack, 1993; Guyot and Reynard, 1992). The existence of $MgSiO_3$-high-clinoenstatite was confirmed by Angel et al. (1992), however, no compression experiment has been reported.

Serghiou and Hammack (1993) reported by *in-situ* X-ray diffraction measurements that $CaSiO_3$-wollastonite underwent a pressure-induced amorphization at 25.6 GPa and no drastic changes of diffraction profiles were observed below the pressure. They suggested that some kinds of defects (*e.g.* extensive stacking fault etc.) introduced by the transformation between polytypes of $CaSiO_3$-wollastonite (Trojer, 1969, Henmi et al., 1978 etc.) lead to the amorphization.

The proposed mechanism of a pressure-induced amorphization of $CaSiO_3$-wollastonite (Serghiou and Hammack, 1993) is controversial, because the transformation between polytypes of $CaSiO_3$ results in no coordination change and also it has been unclear whether the relation of stability fields of each polytype has such a function of thermodynamical parameters as pressure and temperature. It is well known that free energy of each polytype is almost comparable but the energy barrier between each polytype is extremely high.

If a pressure-induced amorphization can be understood as a precursor phenomenon of the transition to some high pressure stable phase, it is required that a high pressure polymorph of $CaSiO_3$ exists. Such high pressure phase may have perovskite-form in consideration of the present experimental result of $CaGeO_3$. $CaSiO_3$-wollastonite transforms to an amorphous state with increasing pressure. On the other hand, $CaGeO_3$-wollastonite transforms to perovskite

form through some phase. This discrepancy may be explained by the proposed interpretation of the present study. The nucleation and growth of $CaSiO_3$-perovskite is quite sluggish. There is an evidence that $CaSiO_3$-perovskite in unquenchable but $CaGeO_3$-perovskite is quenchable.

Recently Hemmati et al. (in press, 1994) found an intermediate crystalline phase with Ca in eight-fold coordination and Si in a pseudo five-coordinated site on the way of the crystal-to-amorphous transition in perovskite-form of $CaSiO_3$ on decompression by lattice dynamical calculations and molecular dynamics simulations. They proposed that similar instability features may also allow a pressure-induced amorphization.

Guyot and Reynard (1992) observed recovered samples of Mg_2SiO_4-olivine from high pressures by TEM and indicated that Mg_2SiO_4-forsterite undergoes a crystal-to-amorphous transition over the pressure above 70 GPa. Although generally transition pressures of silicates are higher than that of germanates, the predicted pressure of the onset of amorphization seems to be too high, as compared with Mg_2GeO_4. In addition, there is a possibility that some high pressure phase was transformed into the amorphous state in decompression process. On the other hand, the MD calculation data of Mg_2SiO_4-olivine indicated that a pressure-induced amorphization may occur at about 40 GPa (Dejima, 1994). *In-situ* observation of a pressure-induced amorphization of Mg_2SiO_4-olivine has never been reported.

Raman study up to 50 GPa (Durben et al., 1993) shows no evidence of a pressure-induced modification and amorphization of Mg_2SiO_4-olivine. *In-situ* X-ray diffraction data on metastably compressed forsterite are available only to 29.5 GPa (Will et al., 1986).

As mentioned above, it is unclear that the silicate olivine and pyroxene

undergo the pressure-induced amorphization at room temperature. However, similar structural modifications take place on both silicate and germanates at kinetically low temperature, because it is probable that the coordination change becomes a major mechanism of compression.

5.4.3 *Comparison with shock loading experiments*

Williams et al. (1990) pointed out the crystalline substances achieved by metastable static compression of silicates may be similar to those accessed on shock loading. Amorphous phases formed by shock waves are commonly observed in shocked meteorites (*e.g.* Milton and De Carli, 1963). Maskelynite and diaplectic glass are their typical examples. They have higher refractive index and density than ordinary glass of the same composition and does not show sharp X-ray diffraction lines (*e.g.* Arndt et al., 1971).

Williams et al. (1990) suggested that the 'mixed phase regime' of the Hugoniot may correspond to the pressure-induced amorphous state. Mashimo et al. (1980), Williams and Jeanloz (1989) and McQueen et al. (1967) reported that Fe_2SiO_4-fayalite and $CaAl_2Si_2O_8$-anorthite amorphizes in static experiments at the same pressure as the onset of the 'mixed phase regime' in shock loading experiments. They also considered that the 'mixed phase regime' is a mixture of a low pressure phase and its high pressure phase. An important similarity between static compression at kinetically low temperature and dynamic compression is that a transition under such conditions does not always take place under an equilibrium condition. In particular, a reconstructive transition and a disproportionation are expected to be difficult to take place without diffusion process of atoms.

According to the Hugoniot data of enstatite (Jeanloz and Ahrens, 1977),

the Hugoniot changes from pyroxene to perovskite through a wide range of mixed phase region. The Hugoniot of forsterite (Jeanloz and Ahrens, 1977) is transformed into mixture of perovskite+magnesiowustite through a mixed phase region. If the results of Hugoniot measurements can be applied to interpretations of static metastable compression experiments, the pressure-induced amorphization observed on the olivine-form should not be a precursor phenomenon of the transition to the spinel-form, but should be a precursor of decomposition to $MgGeO_3$-polymorph and rock salt structure. Silicate-pyroxene should be transformed into the perovskite-form by static compression at kinetically low temperature. However, there have been no static compression data at kinetically low temperature for enstatite.

It is an interesting suggestion how the spinelloid of olivine polymorph might be produced with laboratory shock experiments (Furnish and Brown, 1986), although β and γ spinel crystals have been observed in some meteorites and these may have been formed by the shock waves that accompany meteoritic impact (*e.g.* Madon and Poirier, 1983). The result of static compression experiments of olivine at room temperature (*e.g.* William et al., 1990) indicated that a phase having six-fold Si (or Ge) atoms is expected to appear after the amorphous state. The spinelloid having four-fold Si (or Ge) atoms may not be a post amorphous phase. These evidence may indicate that this mechanism and/or kinetic problems play an important role on both static compression process at room temperature and on experimental dynamic compression process.

6. Conclusions

The transformation of $CaGeO_3$-wollastonite, $MgGeO_3$-high-clinoenstatite and Mg_2GeO_4-olivine were investigated under high pressure at room temperature by *in-situ* X-ray diffraction measurements using the diamond anvil cell (DAC). The three germanates were selected as samples in this study on the basis of the difference in the oxygen packing mode (CCP or HCP).

$CaGeO_3$-wollastonite is transformed into the rhodonite structure at about 6 GPa at room temperature and is recovered metastably at ambient pressure. Samples synthesized at room temperature and at the pressure of 6, 20 and 26 GPa were assigned as the rhodonite-form and the measured density (3.95 g/cm^3) is in good agreement with the calculated density of hypothetical rhodonite-form of $CaGeO_3$. The *in-situ* X-ray diffraction measurements were also conducted under high pressure and moderate temperature (from room temperature to 750°C) on $CaGeO_3$-wollastonite using a cubic anvil type apparatus (MAX80) installed at the National Institute for High Energy Physics in Tsukuba. The $CaGeO_3$-rhodonite becomes unstable above 450°C. Therefore, the rhodonite-form is considered as a thermodynamically metastable phase. Above 15 GPa the rhodonite structure is changed to the phase with a modified perovskite structure, and is further transformed into the orthorhombic $CaGeO_3$-perovskite in the decompression process from 27 GPa to ambient pressure.

Another phase transformation under high pressure at room temperature has been also investigated on $MgGeO_3$-high-clinoenstatite having the same oxygen packing mode (CCP) as the wollastonite-form. $MgGeO_3$-high-clinoenstatite converts to a phase having an unidentified diffraction pattern at about 23 GPa and room temperature. This new phase is different from the ilmenite-form, the $LiNbO_3$-form and the perovskite-form, concluding by the

present diffraction data. This unidentified phase is reversibly transformed into the high-clinoenstatite-form in the decompression process.

Mg_2GeO_4-olivine has the different oxygen packing mode (HCP) from that of the wollastonite-form and the high-clinoenstatite-form. All diffraction peaks of Mg_2GeO_4-olivine disappears in the pressure range from 25 GPa to 30 GPa. This result confirms that a pressure-induced amorphization takes place below about 30 GPa. The amorphization of Mg_2GeO_4-olivine is irreversible transition, because no diffraction peaks appear in the decompression process, even at ambient pressure.

The different compression mechanisms work on the three germanates, according to the comparison between the bulk modulus and the polyhedral bulk moduli. The compression of $CaGeO_3$-wollastonite, $MgGeO_3$-high-clinoenstatite and Mg_2GeO_4-olivine are controlled by the compression of CaO_6 octahedra, the homogeneous compression of constituent polyhedra and a combination of metal-oxygen and oxygen-oxygen compression, respectively.

The agreement of the onset pressure, at which some changes occur, between the present diffraction data and the previously reported XAFS data, suggests that some modifications of long range order of all the three germanates under high pressure at room temperature are motivated by the coordination change of Ge atoms. Only Mg_2GeO_4-olivine undergoes the pressure-induced amorphization, although the other two compounds, which are built of CCP oxygen atoms, are transformed into metastable high pressure phases without showing the amorphization.

The present experiments are interpreted that the pressure-induced amorphization is regarded as a precursor phenomenon during the transition to a high pressure phase and the appearance of "X-ray amorphous" state is not a

thermodynamical but a kinetic process. When the change of the coordination of Ge atoms results in breaking the long range order of a low pressure phase and the nucleation and growth of a high pressure phase is sluggish, the amorphous state is observed by the diffraction technique. On the other hand, when the coordination change does not lead to catastrophic collapse of the long range order and the transition to a high pressure phase progresses rapidly, the amorphization may not be observed. The two kinetic factors relate to the oxygen packing mode and can be described as the following: (1) the conversion rate of the structural transition induced by the modification of the local structure in a low pressure phase and (2) the nucleation and the growth rate of a high pressure phase.

Acknowledgments

I am very grateful to Prof. T. Yamanaka for helpful advice and continuous encouragements throughout this study and to staffs of Department of Earth and Space Science, Osaka Univ. for fruitful discussion.

I thank also Prof. E. Ito of Institute for Study of the Earth's Interior, Okayama Univ. for the opportunities of high pressure experiments using an uniaxial split sphere type apparatus, Prof. T. Yagi of Institute for Solid State Physics, Univ. of Tokyo for supporting high pressure experiments using a DAC, Prof. O. Shimomura and Prof. K. Ohsumi of Photon Factory in National Institute for High Energy Physics for their helpful advice about the X-ray measurements and high pressure experiments using the MAX80 in KEK, Prof. I. Nakai of Tokyo Sci. Univ. for usage of the Berman density torsion balance.

Finally, I would like to thank Prof. H. Takeda of Mineralogical Institute, Univ. of Tokyo for constructive comments on the manuscript.

References cited

Aikawa N. (1979) Oriented intergrowth of rhodonite and pyroxmangite and their transformation mechanism. *Miner. J.*, 9, 255-269.

Akimoto S., and Syono Y. (1972) High pressure transformations in $MnSiO_3$. *Am.. Mineral.*, 57, 76-84.

Andrault D., Madon M., Itie J.P., and Fontaine A. (1992) Compression and coordination changes in pyroxenoids: an EXAFS study of $MgGeO_3$ and $CaGeO_3$ wollastonite. *Phys. Chem.. Minerals,* 18, 506-513.

Angel R.J., Chopelas A., and Ross N.L. (1992) Stability of high-density clinoenstatite at upper-mantle pressure. *Nature*, 358, 322-324.

Arndt J., Hornemann U., and Muller W.F. (1971) Shock wave densification of silica glass. *Phys. Chem. Glasses*, 12, 1-7.

Ballon J., Comparat V., and Pouxe J. (1983) The blade camber: a solution for curved gaseous detectors. *Nucl. Instr.and Meth.*, 217, 213-216.

Baur W.H. (1972) Computer-simulated crystal structures of observed and hypothetical Mg_2SiO_4 polymorphs of low and high density. *Am. Mineral.*, 57, 709-731.

Bernal J.D. (1936) Discussion. *Observatory(London)*, 59, 268.

Decker D.L. (1971) High-pressure equation of state for NaCl, KCl, and CsCl. *J. Appl. Phys.*, 42, 3239-3244.

Dejima M. (1994) Molecular dynamics simulations of the pressure-induced amorphization of forsterite. *master thesis*, 38, Osaka Univ.

Durben D., McMillan P.F., and Wolf G.H. (1993) Raman study of the high-pressure behavior of forsterite (Mg_2SiO_4) crystal and glass. *Am. Mineral.*, 78, 1143-1148.

Fujii Y., Kowaka M., and Onodera A. (1985) The pressure-induced metalic amorphous state of SnI_4: I. A novel crystal-to-amorphous transition studies by X-ray scattering. *J. Phys. C. Solid State Phys.*, 18, 789-797.

Furnish M.D. and Bassett W.A. (1983) Investigation of the mechanism of the olivine-spinel transition in fayalite by synchrotron radiation. *J. Geophys. Res.*, 88, 10333-10321.

Furnish M.D. and Brown J.M. (1986) Shock loading of single-crystal olivine in the 100-200 GPa range. *J. Geophys. Res.*, 91, 4723-4729.

Goldschmidt V. M. (1931) Zur kristallchemie des germaniums. *Nachr. Gesell. Wiss. Gottingen, Math. Phys. Kl. Fachgr.* IV, 1, 184-190.

Guyot F. and Reynard B. (1992) Pressure-induced structural modifications and amorphization in olivine compounds. *Chem. Geol.*, 96, 411-420.

Hazen R.M. (1976) Effects of temperature and pressure on the crystal structure of forsterite. *Am. Mineral.*, 61, 1280-1293.

Hazen R.M. and Finger L.W. (1977) Compressibility and crystal structure of Angra dos Reis fassaite to 52kbar. *Carnegie Inst. Wash. Yearb.*, 76, 512-515.

Hazen R.M. and Finger L.W. (1979) Bulk modulus-volume relationship for cation-anion polyhedra. *J. Geophys. Res.*, 84, 6723-6728.

Hazen R.M., Finger L.W., Hemley R.J., and Mao H.K. (1989) High-pressure crystal chemistry and amorphization of α-quartz. *Solid State Comm.*, 72, 507-511.

Hazen R.M. and Prewitt C.T. (1977) Effects of temperature and pressure on interatomic distances in oxygen-based minerals. *Am. Mineral.*, 62, 309-315.

Hemley R.J., Jephcoat A.P., Mao H.K., Ming L.C., and Mangnani M.H.

(1988) Pressure-induced amorphization of crystalline silica. *Nature*, 334, 52-54.

Hemmati M., Chizmeshya A., Wolf G.H., Poole P.H., Shao J., and Angell C.A. (1994) The crystalline-amorphous transition in silicate perovskite. *Phys. Rev. B*, in press.

Henmi C., Kusachi I., Kawahara A., and Henmi K. (1978) 7*T* wollastonite from Fuka, Okayama Prefecture. *Mineral. Jour.*, 9, 169-181.

Hensen B.J. (1977) Determination of olivine-spinel transition in magnesium germanate (Mg_2GeO_4) up to 20 kilobars and 1300 degree C. *Phys. Earth Planet. Inter.*, 14, P3-P5.

Huang E. and Bassett W.A. (1986) Rapid determination of Fe_3O_4 phase diagram by synchrotron radiation. *J. Geophys. Res.*, 91, 4697-4703.

Hyde B.G., White T.J., O'Keeffe M., and Johnson A.W.S. (1982) Structures related to those of spinel and the β-phase, and a possible mechanism for the transformation olivine ↔ spinel. *Z. Kristallogr.*, 160, 53-62.

Itie J.P., Polian A., Calas G., Petiau J., Fontaine A., and Tolentino H. (1989) Pressure-induced coordination changes in crystalline and vitreous GeO_2. *Phys. Rev. Lett.*, 63, 398-401.

Ito E. and Matsui Y. (1979) High-pressure transformations in silicates, germanates, and titanates with ABO_3 stoichiometry. *Phys. Chem. Minerals*, 4, 265-273.

Jeanloz R. and Ahrens T.J. (1977) Pyroxenes and olivines: Structural implications of shock-wave data for high pressure phases. In *High Pressure Research*, edited by Manghnani M.H. and Akimoto S., 439-461.

Kirfel A. and Neuhaus A. (1974) Zustandsverhalfen und elektrische

Leitfahigkeit von $MgGeO_3$ bei Drucken bis 65kbar und Temperaturen bis 1300°C (mit Folgerungen fur das Druckverhalten von $MgSiO_3$. *Z. Phys. Chem.* Neue Folge 91, 121-152.

Kudoh Y. and Takeuchi Y. (1985) The crystal structure of forsterite Mg_2SiO_4 under pressure up to 149kb. *Z. Kristallogr.*, 171, 291-302.

Kruger M.B. and Jeanloz R. (1990) Memory glass: An amorphous material formed from $AlPO_4$. *Science*, 249, 647-649.

Leinenweber K., Wang Y., Yagi T., and Yusa H. (1994) An unquenchable perovskite phase of $MgGeO_3$ and comparison with $MgSiO_3$ perovskite. *Am. Mineral.*, 79, 197-199.

Liebau F. (1960) Zur Kristallchemie der Silikate, Germanate und Fluoberyllate des Formeltyps ABX_3. *N. Jb. Miner., Abh.*, 94, 1209-1222.

Liebermann R.C. (1974) Elasticity of pyroxene-garnet and pyroxene-ilmenite phase transformations in germanates. *Phys. Earth Planet. Inter.*, 8, 361-374.

Liebermann R.C., Jones L.E.A., and Ringwood A.E. (1977) Elasticity of aluminate, titanate, stannate and germanate compounds with the perovskite structure. *Phys. Earth Planet. Interiors*, 14, 165-178.

Liu L. (1977) Post-ilmenite phases of silicates and germanates. *Earth Planet. Sci. Lett.*, 35, 161-168.

Liu L. and Bassett W.A. (1986) Elements, oxides, and Silicates: High-pressure phases with implications for the earth's interior. *Oxford monographs on Geology and Geophysics No.4*, edited by Liu L. and Bassett W.A., 250, Oxford Univ. Press, New York.

Madon M. and Poirier J.P. (1983) Transmission electron microscope

observation of α, β and γ-$(Mg, Fe)_2SiO_4$ in shocked meteorites: planar defects and polymorphic transitions. *Phys. Earth Planet. Inter.*, 33, 31-44.

Mao H.K. and Bell P.M. (1978) Design and varieties of megabar cell. *Carnegie Inst. Wash. Yearb.*, 904-908.

MashimoT., Kondo K.I., Sawaoka W., Syono Y., Takei H., and Ahrens T.J. (1980) Electrical conductivity measurement of fayalite under shock compression up to 56 GPa. *J. Geophys. Res.*, 85, 1876-1881.

McMahan A.K. (1986) Structural transitions and metallization in compressed solid argon. *Phys. Rev.*, B33, 5344-5349.

McQueen R.G., Marsh S.P., and Fritz J.N. (1967) Hugoniot equation of state of twelve rocks. *J. Geophys. Res.*, 72, 4999-5036.

Meade C. and Jeanloz R. (1991) Deep-focus earthquakes and recycling of water into the earth's mantle. *Science*, 252, 68-72.

Meade C., Jeanloz R., and Hemley R.J. (1992) Spectroscopic and X-ray diffraction studies of metastable crystalline-amorphous transitions in $Ca(OH)_2$ and serpentine. In: *High-Pressure Research: Application to Earth and Planet. Sciences*, edited by Syono Y. and Manghani M. 485-492, TERRAPUB, Tokyo.

Milton D.J., and De Carli P.S. (1963) Maskelynite: formation by explosive shock. *Science*, 140, 670.

Mishima O., Calvert L.D., and Whalley E. (1984) 'Melting ice' I at 77K and 10kbar: a new method of making amorphous solids. *Nature*, 310, 393-395.

Narita H., Koto K., and Morimoto N. (1977) The crystal structures of $MnSiO_3$ polymorphs(rhodonite- and pyroxemangite-type). *Mineral.*

Journ., 8, 329-342.

Ozawa H., Uno R. Yamanaka T., Morikawa H., Ando M., and Ohsumi K. (1988) New powder diffractometer for the photon factory. *Rev. Sci. Instrum.*, 60, 2382-2385.

Pauling L. (1929) The principles determining the structures of complex ionic crystals. *J. Am. Chem. Soc.*, 51, 1010-1026.

Peacor D. and Prewitt C.T. (1963) Comparison of the crystal structures of bustamite and wollastonite. *Am.. Mineral.*, 48, 588-596.

Piermarini G.J., Block S., and Barnett J.D. (1973) Hydrostatic limits in liquids and solids to 100 kbar. *J. Appl. Phys.*, 44, 5377-5380.

Piermarini G.J., Block S., Barnett J.D., and Forman R.A. (1975) Calibration of the pressure dependence of the R_1 ruby fluorescence line to 195 kbar. *J. Appl. Phys.*, 46, 2774-2780.

Prewitt C.T. and Sleight A.W. (1969) Garnet-like structures of high-pressure cadmium germanate and calcium germanate. *Science*, 163, 386-387.

Reynard B., Petit P.E., Guyot F., and Gillet P. (1994) Pressure-induced structural modifications in Mg_2GeO_4-olivine: a Raman spectroscopic study. *Phys. Chem. Mineral.*, 20, 556-562.

Richard G. and Richet P. (1990) Room-temperature amorphization of fayalite and high-pressure properties of Fe_2SiO_4 liquid. *Geophys. Res. Lett.*, 17, 2093-2096.

Ringwood A.E. (1956) The system Mg_2SiO_4-Mg_2GeO_4. *Am. J. Sci.*, 254, 707-711.

Ringwood A.E. and Seabrook M. (1962) High-pressure transition of $MgGeO_3$ from pyroxene to corundum structure. *J. Geophys. Res.*, 67,

1690-1691.

Ringwood A.E. and Seabrook M. (1963) High-pressure phase transformations in germanate pyroxenes and related compounds. *J. Geophys. Res.*, 68, 4601-4609.

Ross N.L., Akaogi M., Navrotsky A., Susaki J., and McMillan P. (1986) Phase transitions among the $CaGeO_3$ polymorphs (wollastonite, garnet, and perovskite structures): Studies by high-pressure synthesis, high-temperature calorimetry, and vibrational spectroscopy and calculation. *J. Geophys. Res.*, 91, 4685-4696.

Ross N.L. and Navrotsky A. (1988) Study of the $MgGeO_3$ polymorphs (orthopyroxene, clinopyroxene, and ilmenite structures) by calorimetry, spectroscopy, and phase equilibria. *Am. Mineral.*, 73, 1355-1365.

Sankaran H., Sikka S.K., Sharma S.M., and Chidambaran R. (1988) Pressure-induced noncrystalline phase of $LiKSO_4$. *Phys. Rev. B Condens. Matter*, 38, 170-173.

Sasaki S., Prewitt C.T., and Liebermann R.C. (1983) The crystal structure of $CaGeO_3$ perovskite and the crystal chemistry of the $GdFeO_3$-type perovskites. *Am. Mineral.*, 68, 1189-1198.

Serghiou G.C. and Hammack W. (1993) Pressure-induced amorphization of wollastonite ($CaSiO_3$) at room temperature. *J. Chem. Phys.*, 98, 9830-9834.

Shimomura O., Yamaoka S., Yagi T., Wakatsuki M., Tuji K., Fukunaga O., Kawamura H., Aoki K., and Akimoto S. (1984) Multi-anvil type X-ray apparatus for synchrotron radiation. *Mat. Res. Soc. Symp. Proc.*, 22, 17-20.

Shimomura O., Yamaoka S., Yagi T., Wakatsuki M., Tuji K., Kawamura H., Hamaya N., Fukunaga O., Aoki K., and Akimoto S. (1985) Multi-anvil type X-ray system for synchrotron radiation. In: *Solid State Physics under Pressure: Recent Advance with Anvil Devices*, edited by Minomura S., 351-356, KTK/Reidel, Tokyo/Dortrecht.

Skelton E.F., Kirkland J., and Qadi S.B. (1982) Energy-dispersive measurements of diffracted synchrotron radiation as a function of pressure: Applications to phase transitions in KCl and KI. *J. Appl. Crystallogr.*, 15, 82-88.

Stolper E.M. and Ahrens T.J. (1978) On the nature of pressure-induced coordination changes in silicate melts and glasses. *Geophys. Res. Lett.*, 14, 1231-1233.

Susaki J., Akaogi M., Akimoto S., and Shimomura O. (1985) Garnet-perovskite transformation in $CaGeO_3$: in-situ x-ray measurements using synchrotron radiation.*Geophys. Res. Lett.*, 12, 729-732.

Trojer F.J. (1969) The crystal structure of a high-pressure polymorph of $CaSiO_3$. *Z. Kristallogr.*, 130, 185-206.

Tsuneyuki S., Matsui Y., Aoki H., and Tsukada M. (1989) New pressure-induced structural transformations in silica obtained by computer simulation. *Nature*, 339, 209-211.

Will G., Hoffbauer W., Hinze E., and Lauterjung J. (1986) The compressibility of forsterite up to 300kbar measured with synchrotron radiation. *Physica B*, 139-140, 193-197.

Williams Q. and Jeanloz R. (1989) Static amorphization of anorthite at 300K and comparison with diaplectic glass. *Nature*, 338, 413-415.

Williams Q., Knittle E., Reichlin R., Martin S., and Jeanloz R. (1990)

Structural and electronic properties of Fe_2SiO_4-fayalite at ultrahigh pressures: Amorphization and Gap Closure. *J. Geophys. Res.*, 95, 21549-21563.

Will G. and Lauterjung J. (1987) The kinetics of the pressure induced olivine-spinel phase transition Mg_2GeO_4. In: *High-Pressure Res. Mineral Phys.* edited by Manghani M. and Syono Y., 177-186, TERRAPUB, Tokyo.

Wolf G.H., Wang S., Herbst C.A., Durben D.J., Oliver W.F., Kang Z.C., and Halvorson K. (1992) Pressureinduced collapse of the tetrahedral framework in crystalline and amorphous GeO_2. In: *High-Pressure Research: Application to Earth and Planet. Sciences*, edited by Syono Y. and Manghani M., 503-517, TERRAPUB, Tokyo.

Yagi T. and Akimoto S. (1982) Rapid X-ray measurements to 100 GPa range and static compression of α-Fe_2O_3. In: *High-Pressure Research in Geophysics.*, edited by Akimoto S. and Manghnani M.H.,81-91, TERRAPUB, Tokyo.

Yamanaka T., Hirano M., and Takeuchi Y. (1985) A high temperature transition in $MgGeO_3$ from clinopyroxene (*C2/c*) type to orthopyroxene (*Phca*) type. *Am. Mineral.*, 70, 363-374.

Yamanaka T., Kawasaki S., and Shibata T. (1992a) Time-resolved observations of solid reactions and structure transitions using a PSD, an SSD and computer aided measurement and control. In:*Advances in X-ray Analysis, Vol.35*, edited by Barrett C.S. et al., 415-423, Plenum Press, New York.

Yamanaka T., Shibata T., Kawasaki S., and Kume S. (1992b) Pressure induced amorphization of hexagonal GeO_2. In: *High-Pressure*

Research: Application to Earth and Planet. Sciences, edited by Syono Y. and Manghani M., 493-501, TERRAPUB, Tokyo.

Yamanaka T. (1994) Geophysical meaning of the pressure-induced amorphization. *J. Mineral. Soc. Japan*, 23, 59-68.

Yamaoka S., Fukunaga O., Shimomura O., and Nakazawa H. (1979) Versatile type miniature diamond anvil high-pressure cell. *Rev. Sci. Instrum.*, 50, 1163-1164.

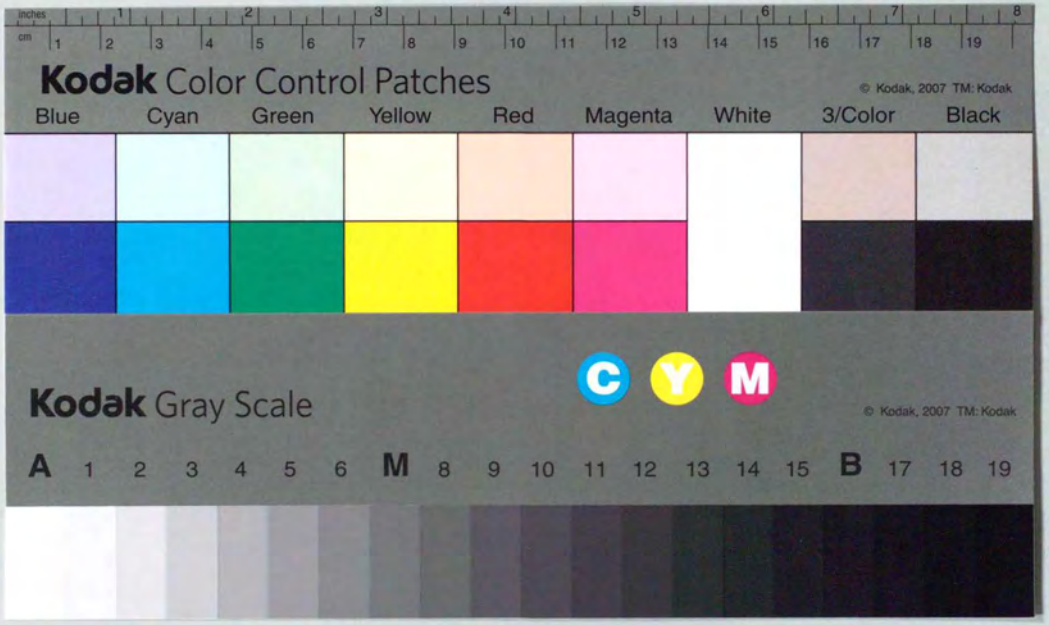
inches
cm
Kodak Color Control Patches
© Kodak, 2007 TM: Kodak
Blue
Cyan
Green
Yellow
Red
Magenta
White
3/Color
Black
C
Y
M
Kodak Gray Scale
© Kodak, 2007 TM: Kodak
A 1 2 3 4 5 6 M 8 9 10 11 12 13 14 15 B 17 18 19